Final Report

EOARD Contract # 2044p
ISTC 00-7036

"Novel asymmetric III-V/II-VI hybrid heterostructures for high power mid-infrared lasers"

Principal Investigator: *Yury P. Yakovlev,*
Dr. Sci., Prof,

Vice-Director
of A.F.Ioffe
Physico-Technical Institute *Andrei G.Zabrodsky,*
Dr. Sci., Prof,

Work period: ***12 months (June, 1, 2001--May, 31, 2002)***

Ioffe Physico-Technical Institute
Saint- Petersburg
Russia

2002

REPORT DOCUMENTATION PAGE

Form Approved OMB No. 0704-0188

1. AGENCY USE ONLY (Leave blank)	2. REPORT DATE	3. REPORT TYPE AND DATES COVERED
	1 June 2002	Final Report

4. TITLE AND SUBTITLE

Novel Asymmetric III-V/II-VI Hybrid Heterostructures For High-Power Mid-Infrared Laser

5. FUNDING NUMBERS

ISTC Registration No:

6. AUTHOR(S)

Dr. Yury Yakovlev

7. PERFORMING ORGANIZATION NAME(S) AND ADDRESS(ES)

Ioffe Institute
26 Polytechnicheskaya St
St. Petersburg 194021
Russia

8. PERFORMING ORGANIZATION REPORT NUMBER

N/A

9. SPONSORING/MONITORING AGENCY NAME(S) AND ADDRESS(ES)

EOARD
PSC 802 BOX 14
FPO 09499-0200

10. SPONSORING/MONITORING AGENCY REPORT NUMBER

ISTC 00-7036

11. SUPPLEMENTARY NOTES

12a. DISTRIBUTION/AVAILABILITY STATEMENT

Approved for public release; distribution is unlimited.

12b. DISTRIBUTION CODE

A

13. ABSTRACT (Maximum 200 words)

This report results from a contract tasking Ioffe Institute as follows: The main objectives of the proposal include technological, structural, theoretical and electro-optical studies of the novel asymmetric III-V/II-VI hybrid heterostructures and fabrication of these structures as mid-infrared lasers. We are proposing a new physical approach consisting of combining III-V and II-VI compounds in the one hybrid asymmetric laser structure based on Al(Ga)SbAs/InAs/Cd(Mg)Se which will lead to large conduction and valence band offsets (in excess of 1 eV for both cases) providing strong carrier and good optical confinement. It will provide suppression of carrier losses from the active region of the laser and leads to better quantum efficiency and weaker temperature dependence of the threshold current of the new laser structure. Additionally, as an alternative approach, GaInAsSb/InAsSbP asymmetric laser structures with high P content (more than 40%) will be grown by MOCVD and studied. Theoretical calculations of this new laser design will be performed. The main parameters of the novel hybrid III-V/II-VI mid-IR laser structure (temperature dependence of threshold current, spontaneous and coherent emission spectra, optical power in pulsed and cw mode) will be investigated. Such lasers should have applications to optical communication through the atmosphere, and materials processing.

14. SUBJECT TERMS

Electrotechnology & Fluidics, Electro-optical & Optoelectronic Devices, EOARD

15. NUMBER OF PAGES
54

16. PRICE CODE
N/A

17. SECURITY CLASSIFICATION OF REPORT	18. SECURITY CLASSIFICATION OF THIS PAGE	19, SECURITY CLASSIFICATION OF ABSTRACT	20. LIMITATION OF ABSTRACT
UNCLASSIFIED	UNCLASSIFIED	UNCLASSIFIED	UL

Key persons:

Maya P. Mikhailova, Deputy P.I., Dr.Sci., p.r.s.
Albert N. Imenkov, Dr.Sci., l.r.s.
Sergei V. Ivanov, Ph.D., l.r.s.
Andrei M. Monakhov, Ph.D., s.r.s.
Konstantin D. Moiseev, Ph.D., s.r.s.
Victor A. Solov'ev, Ph. D., s.r.s.

Investigators:

Yakov V. Terent'ev, Ph.D., s.r.s.
Boris A. Matveev, Ph. D., s.r.s.
Boris Ya. Meltzer, s.r.s.
Sergey V. Sorokin, r.s.
Irina V. Sedova, r.s.
Anastasia P. Astakhova, j.r.s.
Tatyana I. Kachalova, eng.

p.r.s. principal research scientist
l.r.s. leader research scientist
s.r.s. senior research scientist
r.s. research scientist
j.r.s. junior research scientist

List of contents

I. Introduction

High-power mid-infrared semiconductor lasers are of great importance for many applications such as laser diode spectroscopy, pollutant monitoring, low-losses optical communication, medical diagnostics etc. [1-5]. Narrow gap III-V heterostructures are very attractive for this purpose due to simple enough fabrication technology and much higher optical power than that obtained in lead-salt based lasers [6]. On the other hand narrow-gap III-V lasers have some disadvantages due to non-radiative recombination losses, intravalence band absorption, carrier leakage from an active region [7-9].

Recently we proposed some new physical approaches to designing an energy band structure of mid-infrared lasers to improve their parameters. One of them consists in using a type II broken-gap heterojunction in the active region of the laser to suppress Auger-recombination at the interface and to reduce injection current [10]. Type II InGaAsSb/InAsSbP heterostructures were grown by liquid phase epitaxy (LPE) on p-InAs substrate, and a 3.26 μm (80K) laser with improved temperature performance was fabricated [11].

In the framework of preceding project (EOARD Contract F-61775-99-WE016) we proposed a new theoretical model of laser structure with high (more than 3-5 kT) asymmetric barriers for electrons and holes at the interfaces between a narrow-gap quantum well (QW) active layer and wide-gap cladding layers, which can combine the advantages of both type I and type II lasers [12-14]. In the structure the type I QW active layer is sandwiched between wide-gap N- and P-cladding materials forming a type II heterojunction. This approach allows reducing the carrier leakage from the active region of the laser structure, especially hole leakage.

There exist only three III-V compounds to design the proposed laser structures, which could provide high enough barriers for electrons and holes simultaneously: Al(Ga)Sb-InAs-InP. However, the latter is strongly lattice-mismatched to the former two, making the growth of the pseudomorphic III-V laser structure with a strong hole confinement in the InAs active layer to be a very sophisticated task for any of state-of-art technological methods: LPE, molecular beam epitaxy (MBE) or metalorganic vapor phase epitaxy (MOVPE).

In this project we propose a new approach consisting in combining III-V and II-VI compounds in one Al(Ga)SbAs/InAs/Cd(Mg)Se laser heterostructure, which allows one

1. to achieve the necessary large conduction (ΔE_C) and valence band (ΔE_V) offsets (in excess of 1.0 eV for both cases), providing strong carrier confinement;

2. to keep the whole structure pseudomorphic, because CdMgSe solid solution can be completely lattice-matched to InAs;
3. to provide excellent optical confinement due to the large difference in refractive index between the III-V active region (n_{InAs} =3.4) and the II-VI barrier (n_{CdSe}=2.55).

Among the well known and widely used II-VI/III-V heteropairs providing almost perfect lattice matching, like ZnSe/GaAs [15] and CdTe/InSb [16], the CdSe/InAs one still remains unstudied, despite cubic (zinc blende) CdSe layers grown by MBE on a GaAs substrate have been studied [17]. Optical and structural properties of bulk melt-grown hexagonal CdMgSe crystals have been reported as well [18]. As the possible problem in the growth of hybrid structures, one should note a difficulty in formation of high-quality InAs/Cd(Mg)Se interface free from the extended defects (like stacking faults and misfit dislocations) which could diminish significantly laser characteristics.

However, we have fabricated the first hybrid AlSb/InAs/CdMgSe diode heterostructures using two separate MBE chambers [13]. An intense photo- and electroluminescence over 3 μm was observed in the structures at both low (77K) and room temperature [19,20]. Weak temperature dependence of spontaneous emission indicates the effective carrier confinement in the InAs layer due to high potential barriers in conduction (ΔE_C =1.28 eV) and valence (ΔE_V~1.6 eV) bands.

Additionally, as an alternative way, the project will include fabrication and study of InGaAsSb/InAsSb/InPSb laser structures with asymmetric band offsets, which will be grown by MOVPE. The high phosphorous content (up to 60%) in the InPSb cladding layer for composition lattice matched to InAs will provide effective confinement for holes on InAsSb/InPSb heterojunction. To achieve the necessary large conduction band offset ($\Delta E_C \cong 0.6$ eV) for electron confinement the GaInAsSb solid solution will be used.

Thus, main objectives of the proposed project are the technological, structural and electro-optical study of the novel asymmetric III-V/II-VI hybrid heterostructures and fabrication on their basis of high-power mid-infrared lasers.

1.1. Scope of Activities

This project is aimed on fabrication and fundamental studies of new asymmetric III-V/II-VI hybrid heterostructures promising for the development of high-power mid-IR lasers. These lasers are of great interest for many applications including pollutant monitoring, laser spectroscopy, medical diagnostics etc. The fulfillment of the project will certainly promote integration of Russian scientists into the international scientific community. That also meets ISTC goals and objectives.

This project is aimed on fabrication and fundamental studies of new asymmetric III-V/II-VI hybrid heterostructures promising for the development of high-power mid-IR lasers. These lasers are of great interest for many applications including pollutant monitoring, laser spectroscopy, medical diagnostics etc. The fulfillment of the project will certainly promote integration of Russian scientists into the international scientific community.

Main objectives of the proposed Project are creation of a new hybrid III-V/II-VI asymmetric laser structures grown by MBE and design of high-power mid-infrared lasers for the spectral range 3-4 μm. As alternative way, MOCVD growing and study of (Ga) InAsSb/InGaAsSb/InAsSbP laser structures with high P contact will be made.
The following tasks will be carried out:

Task 1 Study and development of MBE growth (growth temperature, flux ratio, doping of the wide-gap claddings) of a novel asymmetric AlGaAsSb/InAs/Cd(Mg)Se hybrid heterostructures emitting in mid-infrared (3-5 μm) region. Main efforts will be focused on solving the problem of formation of uniform high quality III-V/II-VI interfaces with low defect density (optimization of InAs surface reconstruction and CdSe growth initiation procedure), providing high quantum efficiency of the structures. XRD, SEM, SIMS, EBIC and TEM methods will be employed for study of InAs/(Cd,Mg)Se and CdSe/CdMgSe heterointerface quality.

Task 2 Hybrid AlAsSb/InAs/CdSe/Cd(Mg)Se laser diode heterostructures will be fabricated by MBE on p-InAs substrate and studied in dependence on thickness and doping level of AlGaAsSb claddings. Post-growth technology (photolitography and manufacturing of Ohmic contacts) for the top n-(Cd,Mg)Se layers will be developed.

Task 3 Photoluminescence and electroluminescence measurements of the grown structures in dependence on growth condition, doping level of confinement layers and the active region thickness will be carried out. Careful experimental and theoretical examination of the type of the heterojunction (I or II) and the band offset values will be performed for the InAs/CdSe, CdSe/CdMgSe, and AlGaSbAs/InAs interfaces.

Task 4 Alternative III-V laser diode structures with asymmetric band offsets based on InGaAsSb/InAsSbP/InPSb with high phosphorous content (P>69%) will be grown by MOCVD and investigated.

Main laser parameters of both type laser structures (threshold current, characteristic temperature, quantum yield, spontaneous and lasing spectra, optical power both in pulsed and cw mode) will be measured in a wide temperature range.

1.2. Technical Schedule

Quarter I.

Study and development of molecular beam epitaxy (MBE) growth of novel asymmetric AlGaSbAs/InAs/Cd(Mg)Se hybrid hetero-structures emitting in mid-infrared (3-4μm) region.

1.1. Growth of the AlGaSbAs layers lattice-matched to InAs substrates.

1.2. Growth of the CdSe ? CdMgSe layers on InAs. In-situ study of growth initiation stage by reflection high energy electron diffraction (RHEED).

1.3. The MBE growth condition optimization aimed at the realization of homogeneous and high quality III–V/II–VI heteroboundary with low density of defects. Studies of the hybrid heterostructures by characterization techniques: x-ray diffraction, TEM, SEM, EPMA, SIMS.

1.4. Optical measurements of band offsets for the heterojunctions InAs/Cd(Mg)Se and CdSe/CdMgSe.

Quarter II.

Fabrication of hybrid III–V/II–VI diode laser structures by MBE.

2.1. The MBE growth condition optimization (growth temperature, flux ratio, doping of the wide-gap claddings) for the p-i-n AlGaSbAs/CdSe/CdMgSe laser structures grown on p-InAs substrates.

2.2. Investigation of structural and electric (I-V, C-V) characteristics of the structures as dependent on the thickness and doping level of active region and claddings.

2.3. The development of post-growth technology (photolithography of mesa-diodes and Ohmic contacts fabrication) for the n-CdMgSe layers.

2.4. Theoretical calculation of asymmetric AlGaSbAs/InAs/Cd(Mg)Se hybrid heterostructure design with current losses suppression.

Quarter III.

Optical studies of asymmetric hybrid AlGaSbAs/InAs/Cd(Mg)Se laser structures.

3.1. Investigation of photo- and electroluminescence of the structures in the temperature range 77-300K as dependent on the growth conditions, thickness and doping level of active region and AlGaSbAs claddings.

3.2. Theoretical studies of the type of heterojunction and band offsets at InAs/Cd(Mg)Se, CdSe/CdMgSe heteroboundaries as well as comparison of the theoretical and experimental results.

3.3. Study of laser parameters of the hybrid laser structures (temperature dependencies of threshold current, spontaneous and lasing spectra, optical power both in pulsed and cw mode).

3.4. Developing of optimal design of hybrid laser structure.

Quarter VI.

Fabrication and study of asymmetric InGaAsSb/InAsSb/InPSb laser structure by metal-organic vapor-phase epitaxy (MOVPE).

4.1. The development of MOVPE growth technology of InGaAsSb/InAsSb/InPSb laser structures with high phosphorous content (P>60%).

4.2. The development of post-growth technology (photolithography of mesa-diodes, Ohmic contacts) of the structures.

4.3. Optical measurements of band offsets for the heterojunctions InAsSb/InPSb and InGaAsSb/InAsSb.

4.4. Optimization of asymmetric InGaAsSb/InAsSb/InPSb laser structure design.

4.5. Study of laser parameters for the laser structures containing phosphorous (temperature dependencies of threshold current, spontaneous and lasing spectra, optical power both in pulsed and cw mode).

4.6. Comparable analysis of the hybrid and phosphorous containing laser structures.

1.3. Technical approach and methodology

In the project we propose for the first time a new physical approach to designing high-power mid-infrared lasers. It consists in combining III-V and II-VI compounds in one laser Al(Ga)SbAs/InAs/Cd(Mg)Se structure. That allows one to obtain pseudomorphic structures with strong both electron and hole confinement, which emits at wavelength over 3 μm. The hybrid structures will be grown by molecular-beam epitaxy (MBE) sequentially in two separate technology set-ups. Additionally, as an alternative way, the project will include the fabrication by metal-organic vapor phase epitaxy (MOVPE) and study of asymmetric GaInAsSb/InAsSb/InPSb laser structures with high phosphorous content.

Broad spectrum of modern characterization techniques including in-situ RHEED, x-ray diffractometry, TEM, SEM, EPMA, SIMS and photoluminescence will be used to study and optimize the technology of formation of high quality III-V/II-VI interface free from the extended defects.

A set of optical methods (absorption, reflection, luminescence) will be used for band offsets measurements. The experimental data will be compared with results of computer modeling of band alignment. The in-depth investigations of photo- and electroluminescence of the proposed structures in the wide temperature range (77-300K), as dependent on the growth conditions and layers parameters, will be performed.

Development of post-growth technology of mesa-diodes will be carried out on the basis of standard methods of photolithography and vacuum deposition.

1.4. Expected results

1. Novel hybrid III-V/II-VI asymmetric laser heterostructures with high band offset confinement will be grown by two-stage MBE method for the first time.
2. Technological, structural and photoluminescence investigations will be done to study interface quality of III-V/II-VI heteroboundaries. Band offset values for the heterojunctions will be determined by optical study.
3. Theoretical simulation of a new asymmetric hybrid laser desing will be performed and problem of suppression of carrier losses from active region of the new laser structure will be considered.
4. Main parameters of hybrid III-V/II-VI lasers (temperature dependence of threshold current spontaneous and lasing spectra, optical power in pulsed and cw modes) will be studied.

II. Theory and Experimental results

2.1. Theoretical model

New physical concept is in using asymmetrical heterostructure with high band offsets at the interface between an active layer and wide gap confined layers. In this structure a narrow active layer (quantum well or superlattice) sandwiched between wide-gap layers forming type I heterojunction (Fig.1). Wide gap n- and p-layers form type II heterojunction pairs and have Eg higher than photon energy of emission.

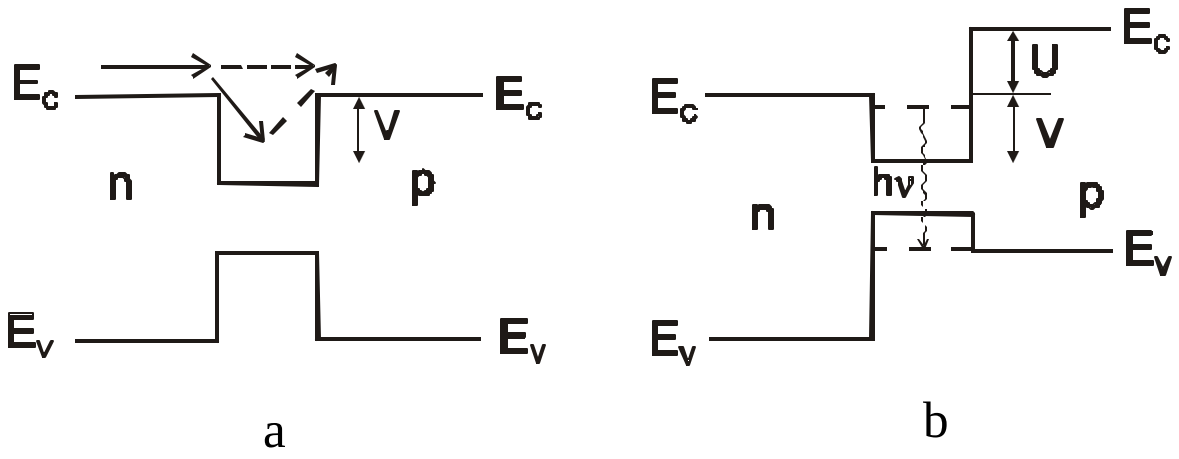

Fig.1. Energy band diagram of mid-infrared laser structure for standard DH-structure (a) and the structure with asymmetric band-offset confinement (b).

In this model asymmetric quantum well is the main feature of new laser. Optical confinement will be made by using wide gap thicker layers (2-3 μm) based on, for example, InAsSbP or GaInAsSb. In such heterostructure a strong overlapping wave functions of electrons and holes at the heteroboundary with an active layer takes place. It leads to the same optical gain as it is in traditional double heterolasers, but by substratial suppression both injection and non-radiative losses. In proposed device a low threshold current and its weak temperature dependence are expected.

To decrease injection losses in an active we propose comparison to standard type I heterostructure shown in Fig.1a. New structure allows to reduce operation current of the laser in comparison to standard type I heterostructure. Indeed, total current is sum of radiative recombination and drift (injection) component. Recombination currents must be the same in the active region of both structures. But as to leakage currents their ratio will be

$$\frac{J_1}{J_2} \approx \left(- \frac{V}{kT_{eff}} \right), \qquad (1)$$

where T_{eff} is effective temperature of an active layer, and V is height of barrier. This current is not high in comparison with recombination current at low temperature and low optical power.

The threshold current is $J_{th}=J_R+J_{leak}$, where J_{leak} is the leakage current which consists of non-radiative recombination current, Auger-current and injection losses which are due to the carriers injection from the quantum well to n- and p-regions:

$$J_{leak} = J_{NR} + J_A + J_{inj}. \qquad (2)$$

If the height of the energy barriers U_1 and U_2, that is equal to (E_{CR}-E_{CN}) for electrons and (E_{VN}-E_{VP}) for holes respectively, are chosen to exceed 3-5 kT at working temperature of the device (200-300K), the last term in the expression for the leakage current can be neglected and the total current is determined only by the recombination one in the narrow-gap region of device. It can be called "non-injection" current, because no current injection through p-n junction occurs. The calculations of the Auger-recombination losses carried out for type II heterojunction[7], which can be used as an estimation for our case, shows that proposed device provides at least the 25 times higher gain in the laser structure with asymmetric band offset confinement (ABOC) with respect to that in a conventional type I heterojunction laser but at the same very low level of the injection losses. The proper QW material selection allows one to reduce also the Auger recombination losses by tuning out of a resonance between the photon energy and the energy gap to a spin-orbit splitted valence band.

Such a unique combination of the advantages of type I and type II heterostructure lasers in one QW ABOC laser structure allows us to believe that the novel ABOC laser under consideration will be able to operate at room temperature at the wavelength in the 3-6 μm range.

The advantages of the proposed QW ABOC laser in comparison with a quantum cascade laser are:

- the higher output power,
- the relative simplicity of fabrication,
- the ability to make a set of lasers for different wavelengths using the same technology and varying the QW width only.

To obtain laser generation a high density of states needs. To reach high power it is important to get real large density of generating centers.

To optimize laser performance, it needs:

1) to reduce of optical losses (for example, by using external resonator). Maximum output power begins to rise linearly with cavity length:

$$P_{output}^{\max} \equiv a_0 l \left(1 - \sqrt{\frac{b}{a_0}} \right)^2 P_S \qquad (3)$$

at reflector transparency

$$T_{opt} = 2a_0 l \left(\sqrt{\frac{b}{a_0}} - \frac{b}{a_0} \right) \qquad (4)$$

2) to reduce electrical losses

3) to reduce non-radiative recombination losses and losses on non-coherent emission (quality of laser structures)

Then “ideal” laser structure must look as the following:

1. Low-dimensional active layer (quantum well, superlattice) with big number of homogeneous emitters.
2. Good optics in design of laser structure (resonators, indices)
3. Decreasing of injection current losses in an active layer.

This approach needs a careful theoretical calculation of the active region parameters to provide an existence of at least one well confined bound state for both types of the carries (electrons and holes) in the QW with asymmetric barrier heights. On the other hand, it is necessary to choose the materials for both the active and confining layers which should be able to form nearly lattice-matched heterostructure and to be grown by the currently available technological equipment (MBE, LPE, MOCVD).

The tentative calculation in a rectangle barrier approximation and not taking into account the complex valence band structure shows that the ABOC device based, for instance, on p-GaAsSb/InAs/n-InP or p-GaAsSb(Al)/InAsSb/n-InAsSbP heterostructures can operate at the room temperature at the wavelength of about 3 μm. These structures can be fabricated either by MBE, by LPE, MOCVD, or by MBE in combination with LPE technology.

Lets consider and compare an ideal model of the conventional laser double heterostructure (Fig.1a) and asymmetric structures (Fig. 1b). For simplicity we will consider the active region of both structures to be the same. Besides, we will suppose that the thickness of an active region is large enough (about 1 μm) as it is usual for LPE grown structures. In this case

we can use the quasi-classical approximation and neglect the quantum-size effects in the active layer.

Let's examine processes in the conduction band (similar processes take place in the valence band). Electrons that fall into an active region from n-region will relax by energy and captured in it, recombining then with holes (radiative or non-radiative), or leaving an active region by activation process. The difference between Fig.1a and Fig.1b is an existence of an additional barrier on the heterointerface of the region with another conductivity type. Such barrier firstly increases to some extent the carrier capture probability by active region due to an existence of a turn-off point at the classical trajectory near the barrier, but it is not very important because the capturing time is small enough even without this barrier. Secondly this barrier reduce the probability of carrier in injection from the active layer to the region with the inverse type of conductivity. The last process is more important and we will consider it in more details. Usually the energy relaxation time is much smaller than the radiative recombination time, so for our estimation we will suppose that there is the quasi-equilibrium in side an active region, with some characteristic temperature T and quasi-Fermi level coinciding approximately to band edge. Further, we suppose that carrier distribution in an active region is usual Fermi distribution. Then energy carrier density (number of carrier divided on the energy interval in the volume unit of an active layer) is:

$$dn(E) = \frac{\sqrt{2}\quad m^{3/2}}{p^{2}\hbar^{3}} \cdot \frac{\sqrt{E}\quad dE}{e^{\frac{e-m}{kT}}+1} \qquad (5)$$

and the connection between the total average carrier density and the Fermi-level position:

$$\overline{n} \equiv \frac{N}{V} = \frac{\sqrt{2}\quad (mT)^{3/2}}{p^{2}\hbar^{3}} \int_{0}^{\infty} \frac{\sqrt{z}\quad dz}{e^{z-\frac{m}{kT}}+1} \qquad (6)$$

Injection losses are determined by the number of electrons, which goes out to the right side from an active layer (See Fig 1). (Electrons going out to the left, in the n-region, are compensated by a proper number of coming electrons and do not contribute in the current in the device). At the same time electrons, which were injected into the p-region, can recombine and thus make some contribution to the total current). A number of these electrons in a time unity will be for the case in Fig. 1a:

$$J_{inj}^{(a)} = \frac{m^{3/2}}{\sqrt{2}\quad p^{2}\hbar^{3}} \int_{0}^{\infty} \frac{\sqrt{x+V}\quad dx}{e^{\frac{x}{kT}}+1}$$

(7)

And for the case in Fig. 1b,

$$J_{inj}^{(b)} = \frac{m^{3/2}}{\sqrt{2}\ \ p^2\hbar^3}\int_u^{\infty}\frac{\sqrt{x+V}\quad dx}{e^{\frac{x}{kT}}+1} \qquad (8)$$

The ratio of these values (3) and (4) will be named efficiency β (T,U,V_0) of the injection suppression of the device (b):

$$b(T,U,V) = 1 - \frac{\int_U^{\infty}\frac{\sqrt{x+V}}{e^{\frac{x}{kT}}+1}dx}{\int_0^{\infty}\frac{\sqrt{x+V}}{e^{\frac{x}{kT}}+1}dx} \qquad (9)$$

Fig.2a shows the temperature dependence of the function $\beta(T,U,V)$. It is evidently that although the injection efficiency decreases with temperature increase, but an injection suppression coefficient is still about 0.6 at room temperature. Now we evaluate decreasing of critical current of devices represented on Fig.1b in comparison with Fig.1a. We present the "pessimistic" estimation of the minimum profit in a critical current, which can be obtained due to additional barriers at the heteroboundary. Let's consider that all carrier with energies lying lower the Fermi level recombined with the same recombination time as carrier inject time over the barrier edge. This hypothesis leads to overestimation of the recombination current, but it is useful as the estimation of the ratio of the injection and the total current. Fig.2b inhibits the temperature dependence of this J_{inj}/J_{tot} ratio. It can be seen that injection current is about 30% from the total current, and using a Fig.1b design allows to reduce a threshold current at least by 20% at room temperature. In the same way some other sufficient values can be easily estimated. In Fig.2b it is shown the temperature dependence of the J_{inj}/J_{tot} ratio for device presented in Fig 1a. Fig.2c shows the same ratio as a function of the quantum well depth at T=300K. At last, in Fig. 2d and Fig.2e we plot the dependence of the efficiency of the injection current suppression as a function of value U and V. Our estimations show that proposed laser structures with asymmetric band offset confinements are effective especially under the following conditions:

a) High operation temperature;
b) b) Additional band offsets are about 2-3 kT;

c) c) Quantum well for carriers is not very deep. In this sense for the band offset of 30 meV in the valence band the injection suppression can be rather effective than for the band-offset in the conduction band of 200 meV.

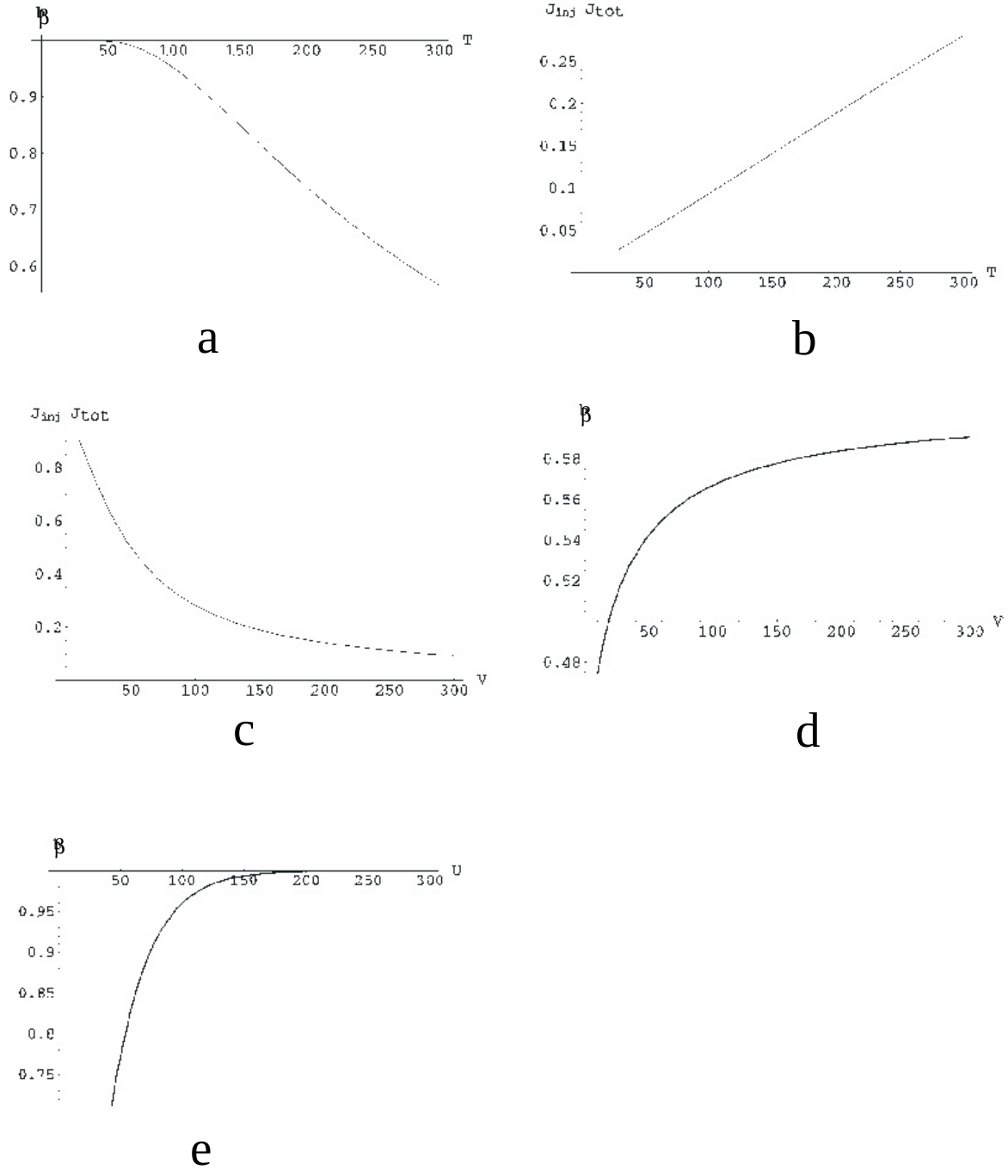

Fig.2 a) The temperature dependence of the injection current suppression for design in Fig 1b with U=100meV and U=30 meV. b) The temperature dependence of the ratio of the injection current to the total current for the design in Fig.1a with V=100meV. c) The dependence of the Jinj/Jtot on well depth design in Fig. 1a at T=300K. d) The dependence of the efficiency of injection current suppression of the well depth V for the structure in Fig.1b with

U=30meV at T=300K. e) The efficiency of injection current suppression as a function of the barrier heigh U for the structure in Fig.1b with U=100 meV at T=300K.

2.2. Study and development of MBE growth of novel asymmetric AlGaAsSb/InAs/Cd(Mg)Se hybrid heterostructures

2.2.1. Growth of the III-V part of the hybrid structures

Growth of the AlGaAsSb layers lattice-matched to InAs

One of the problems to be solved for the III-V part of the hybrid structures is the optimization of molecular beam epitaxy (MBE) growth conditions for AlGaAsSb layers lattice-matched to InAs. An influence of MBE growth parameters (substrate temperature, total group V flux, and As/Sb flux ratio) on a composition of $Al_xGa_{1-x}As_ySb_{1-y}$ alloys (x = 0.5) as well as their structural quality have been studied in details. Using these data, As and Sb incorporation coefficients have been evaluated. The absolute values of As and Sb incorporation coefficients have been found to be much smaller than unity, with the ratio of Sb to As coefficients exceeding 10.

Three series of samples were grown on a RIBER 32P setup equipped with the antimony cracking cell RB-075-Sb providing mostly Sb_2 flux. In each series only one growth parameter is varied (As flux, Sb flux or the substrate temperature - T_S). Both InAs and GaSb substrates were used. The structures contain a 0.2 μm-thick InAs or GaSb buffer layer followed by a (0.5-1) μm-thick $Al_{0.5}Ga_{0.5}As_ySb_{1-y}$ layer. The AlGaAsSb composition was measured by electron probe microanalysis (EPMA) and verified through the simulation of high resolution X-ray diffraction (XRD) rocking curves using the EPMA data on Al and Ga content. Additionally, the compositional profiles of the structures were obtained by secondary ion mass spectroscopy (SIMS).

It was found that As flux variation within a wide range does not affect the composition of AlGaAsSb, provided that it is grown at the Sb_2 flux large enough to keep group V-stabilized growth conditions. The dependencies of arsenic content (y) in the $Al_{0.5}Ga_{0.5}As_ySb_{1-y}$ alloy on antimony beam equivalent pressure (BEP) as well as growth temperature are presented in Fig. 3 and Fig. 4, respectively. The minimum BEP of Sb flux corresponding to Sb-stabilized growth of $Al_{0.5}Ga_{0.5}Sb$ was $1.7 \cdot 10^{-6}$ and $2.2 \cdot 10^{-6}$ Torr at T_S of 480°? and 520°? , respectively, as shown by vertical dashed lines in Fig. 3. In contrast to thermodynamic predictions, the experimental data demonstrate the dominant Sb incorporation into AlGaAsSb layers even at rather low Sb fluxes.

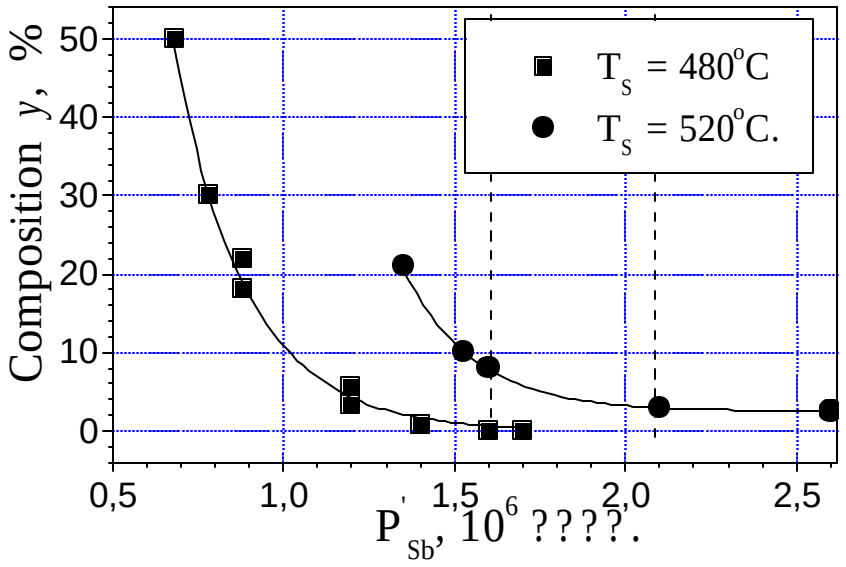

Fig. 3 As content in the $Al_{0.5}Ga_{0.5}As_ySb_{1-y}$ as a function of Sb BEP at two different growth temperatures.

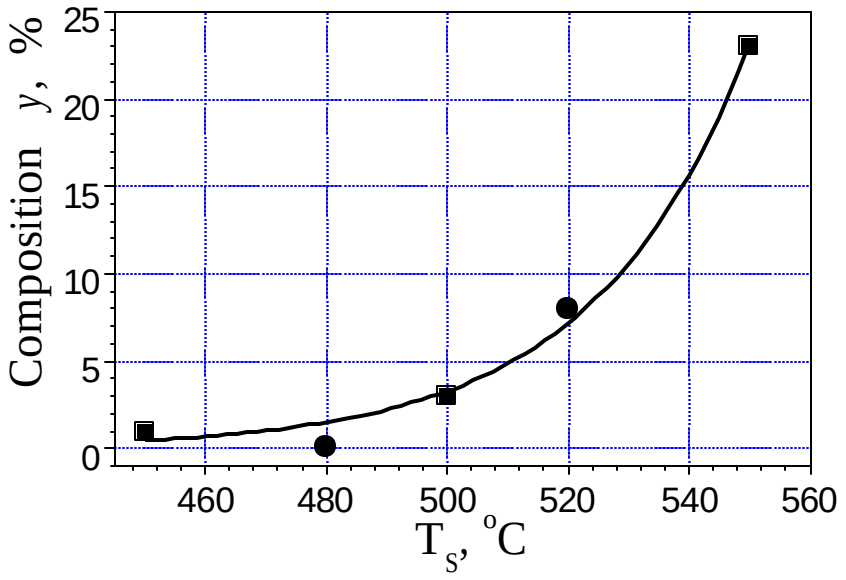

Fig. 4. As content in the $Al_{0.5}Ga_{0.5}As_ySb_{1-y}$ as a function of the growth temperature. The data of this work and of A. Bosacchi *et al.* [J. Cryst. Growth **201/202**, 858 (1999)] are marked by circles and squares, respectively.

Such incorporation behavior of the volatile elements can be explained by a strong difference in kinetically controlled As and Sb incorporation coefficients. Thus, to be correct any thermodynamic model of MBE should take into account the kinetics processes on growth

surfaces. One should note that the samples grown at high growth temperature ($T_S \sim 520°?$) and high V/III ratio (high As flux) demonstrate much worse morphology and structural quality, as demonstrated by XRD rocking curves presented in Fig. 5.

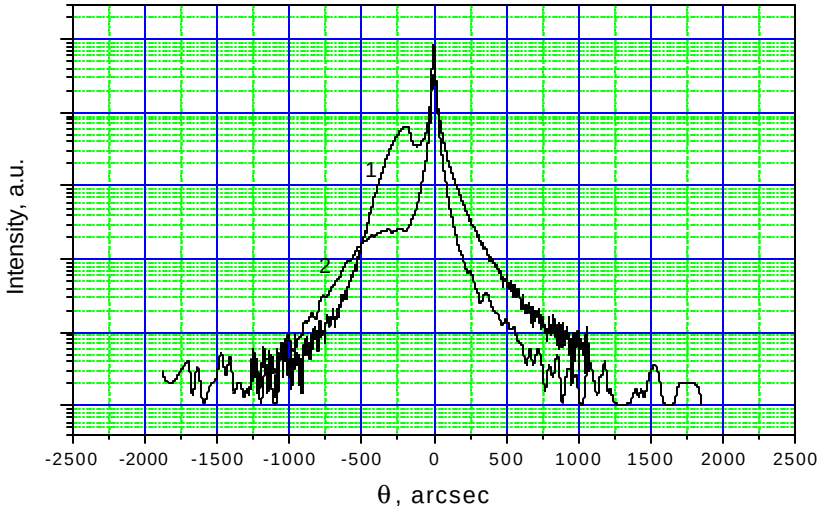

Fig. 5. X-ray diffraction Θ–2Θ rocking curves of the structures with single $Al_{0.5}Ga_{0.5}Sb_{0.89}As_{0.11}$ layers grown at temperature 480°? (1) and 520°? (2).

Finally, both the experimental data and theoretical calculations demonstrate strong dependencies of AlGaAsSb alloy composition on growth temperature and Sb flux. The alloy composition has been found to be efficiently controlled by varying only the Sb flux with Al, Ga, As fluxes and growth temperature kept constant.

2.2.2. Doping of the AlGaAsSb layers

For the hybrid lasers the p-AlGaAsSb doping level of p=(3-5)·10^{17} cm^{-3} seems to be quite reasonable. Beryllium have been used as a p-type dopant for both buffer InAs and AlGaAsSb layers. Calibration of the doping level have been performed using test structures which contained single (0.6-0.8) μm-thick layers (InAs or AlGaAsSb) grown on semi-insulated GaAs (100) substrates, because semi-insulating InAs substrates are not widely spread. The hole concentration of p= (3.5-4)·10^{17} cm^{-3}, reached in AlGaAsSb at the appropriate Be cell temperature, was demonstrated by Hall measurements at room temperature. However, current-voltage characteristics (I-V) measured in the first hybrid laser structures as well as in the structures containing only III-V part of the hybrid heterostructures grown pseudomorphically on InAs

substrates showed rather large series resistance, which indicates much lower doping level of p-AlGaAsSb. The possible reason of such discrepancy is likely a strong defect-induced enhancement of the intrinsic carrier concentration in the AlGaAsSb layers grown on strongly mismatched substrates, like GaAs. Similar effect has been observed previously for InAs/GaAs heterolayers, where the intrinsic electron concentration decreased gradually with an increase in the InAs thickness, i.e. with reduction of a contribution of large defect density generated at the InAs/GaAs interface.

To clarify the situation, we have grown a 0.8 μm-thick AlGaAsSb layer on a compensated InAs substrate with very small electron concentration $n \sim 10^{15}$ cm^{-3}. The Hall parameters measured in this structure at temperature 77 K displayed not hole but electron conductivity and gives the values of electron concentration and mobility $n = 7.5 \cdot 10^{16}$ cm^{-3} and $\mu = 2100$ cm^2/Vs, respectively. These values are supposed to be inherent to electron channel forming at the type II InAs/AlGaAsSb heterojunction. We believe that such electron channel can be formed only if the doping of AlGaAsSb layer is not large enough ($p < 10^{17}$ cm^{-3}), i.e. the Fermi level lies deep in the AlGaSbAs energy gap not far from the InAs conduction band edge. That explains the rather large series resistance in the first hybrid laser structures. As a result, the Be doping level of AlGaSbAs in the following hybrid structures was increased by 5 times.

2.2.3. Growth of the II-VI part of the hybrid structures

Protecting the InAs surface from oxidation in atmosphere

The hybrid structures were grown in two separate MBE setups and transferred from the III-V chamber to the II-VI one through air. We have used two methods for protecting the InAs surface from oxidation in atmosphere: covering with polycrystalline As and a sulfur passivation.

In the former case, after III-V growth, the wafer was covered with an As cap layer deposited during 15 min at a substrate temperature $T_S < 3°C$ and a conventional As_4 beam equivalent pressure and then transferred to the II-VI chamber through air. In the II-VI chamber, the As cover was removed by annealing the sample at T_S= 460-480°C. A RHEED system was used to monitor surface conditions. The II-VI growth initiation conditions corresponded to an intermediate (2×4)As&(4×2)In InAs surface reconstruction achieved at T_S~ 460-480°C.

In the case of the Na_2S passivation, the InAs surface is not expected to contain oxides and is covered with a sulfide protecting overlayer. The samples were immersed in $Na_2S \cdot 9H_2O$ (1M) solution and rinsed in a deionized water. After the In-mounting on the sample holder, the

passivated samples were immediately loaded into “annealing” chamber, which is equipped with an As effusion cell and has air-free connection with the II-VI chamber, for annealing under the As flux. A series of surface reconstructions were investigated using RHEED by increasing the annealing temperature: a disordered S-rich (1x1), ordered S-terminated (2x1) and finally a S-free (4x2) In-terminated surface. A sharp (2x1) reconstruction was found after annealing at 410°C while a disordered (1x1) was found for lower annealing temperatures. Streaky and sharp (4x2) RHEED patterns, transformed to the pure (2x4) one under the As flux, was obtained by increasing T_S to 450°C, resulting in the complete sulfur desorption. After annealing these structures were transferred into the II-VI MBE chamber through the high vacuum.

At this stage the experiments were focused on the study of the surface morphology of the InAs substrates because the damage of the surface substrate morphology induced by the pre-epitaxial annealing has been shown to be the origin of the defect formation in epitaxial overlayer. The typical surface morphology of two group samples: (1) reference, non-passivated, InAs substrates prepared using the chemical treatment procedure, which involves etching in a $1CrO_3$:4HCl:$3H_2O$ solution followed by rinsing in a deionized water, and (2) passivated in the Na_2S solution has been studied by an atomic-force microscopy (AFM) after vacuum annealing in MBE setup. The solution concentration and duration of Na_2S treatment were varied to select the optimal regime. A comparative analysis (see Fig. 6) of the surface morphology after annealing of both group samples shows that proposed sulfide treatment also makes it possible to reduce considerably the surface roughness amplitude. Fig. 4b shows typical AFM images of surface morphology of the passivated sample after annealing. Indeed, atomically flat surface with three atomic steps (cross-section of Fig. 5b) can be seen.

The observed findings are in very good agreement with the very sharp and streaky (2x4)As pattern typical for high quality pure atomically-flat InAs layer surface, resulting in a two-dimensional (2D) initial CdMgSe:Cl growth mode. For the InAs-terminated structures protected in this way the first type of growth initiation procedure was used.

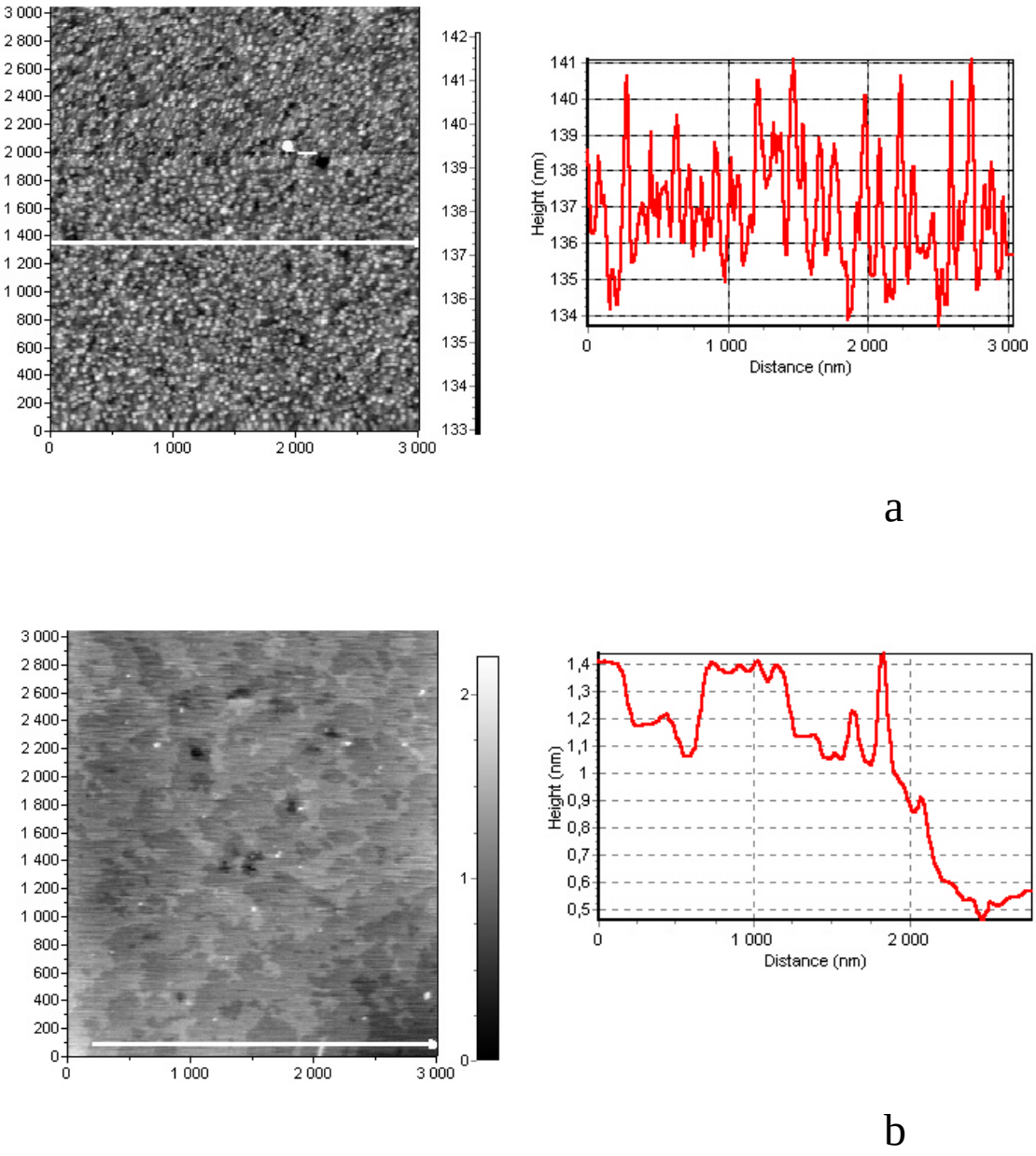

Fig. 6. AFM topography and cross-section images of the InAs sample surface after annealing without (a) and with (b) the S-passivation.

2.2.4. Initiation growth of the II-VI part

The main problem in the MBE growth of II-VI part of the hybrid structures concerns the formation of high quality III-V/II-VI heterointerfaces. Two types of growth initiation procedure at the III-V/II-VI interfaces were used. At the first one, a 10 nm thick CdMgSe layer was grown in a migration enhanced epitaxy (MEE) mode at T_S~200°C to reduce the defects density on the InAs/CdSe interface, by analogy with the GaAs/ZnSe case [J.M. Gaines, J. Petruzzello,

B. Greenberg, J. Appl. Phys. 73, 2835 (1992)], which usually resulted in a streaky (2x1) Se-stabilized RHEED patterns. The deposition times of Cd and Mg were chosen to provide desirable alloy composition. At the other, T_S=280°C was kept constant from the very beginning of II-VI growth which was initiated with a deposition of a ~5 nm thick ZnTe buffer in the MBE mode.

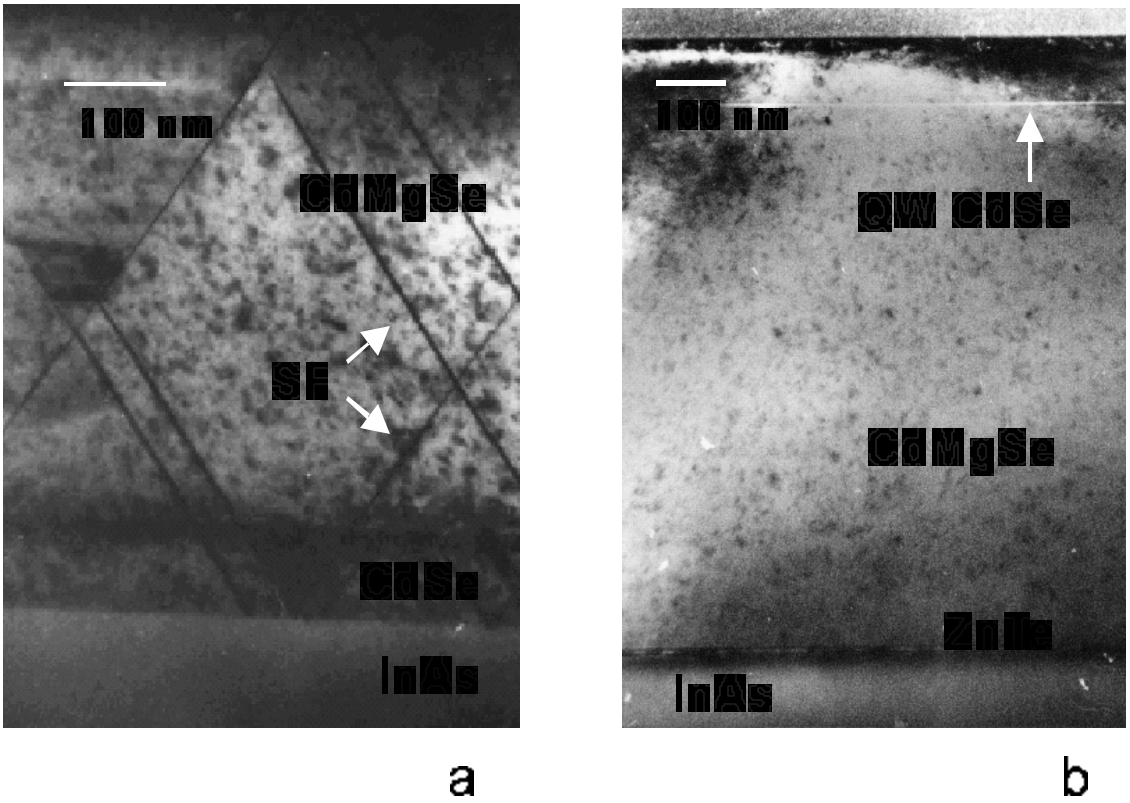

Fig. 7. Cross-sectional TEM images of the CdSe (100nm)/ CdMgSe structures with a CdSe/InAs interface (a) and the 2 nm-CdSe/ CdMgSe QW structure with a ZnTe buffer layer at the III-V/II-VI interface (b).

The growth of the following (Cd,Mg)Se structure occurred at 280°C in the MBE mode under the (2×1) Se-stabilized conditions in both cases. It consists usually of 20 nm of moderately-doped with chlorine n-$Cd_{1-x}Mg_xSe$ with x in between 0.15-0.2, followed by ~1 μm of n-$Cd_{1-x}Mg_xSe$:Cl lattice-matched to InAs (x=0.1) with gradually enhanced doping level from $5x10^{17}$ to $5x10^{18}$ cm^{-3}. Finally, a 100-nm thick n^+-CdSe:Cl contact layer is deposited. The hybrid structures with the two different interface types were studied by cross-sectional TEM (Fig. 7). The structures used As-polycrystalline protection with the InAs/CdSe interface usually exhibit the stacking fault (SF) density around 10^7 cm^{-2}, which is probably due to the not completely

optimized initial surface reconstruction of InAs, allowing an In-Se interaction at the heterovalent InAs/CdSe interface formation. The formation enthalpy (-344 kJ/mole) of In_2Se_3 characterized by a defect sphalerite structure is even smaller than that of Ga_2Se_3, making the probability of In_2Se_3 nucleation at the InAs/CdSe interface very high. Contrary to that, the SF density in the structure with the ZnTe buffer layer (~5 nm) is at least two orders of magnitude lower (below 10^6 cm^{-2}), which is obviously explained by the ZnTe passivation of the InAs surface before a Cd(Mg)Se growth.

Finally, the structures with S-passivated InAs, demonstrating perfect (2x4) As-stabilized RHEED pattern after annealing under As flux, has shown even better 2D growth initiation mode using CdMgSe MEE deposition at 200°C. Preliminary data on RHEED and XRD characterization imply the lower defect density in this case. The MBE growth of CdMgSe layers has been found to be most preferable under the Se-stabilized conditions corresponding to a (2x1) surface reconstruction, that makes easier the alloy composition control varying flux ratio for metals only.

2.2.5. Estimation of band alignment of the hybrid structures

A theoretical estimate of the relative alignment of energy bands in the proposed hybrid heterostructures was made, using transitivity rule and "model solid theory" of Van de Walle [Phys. Rev. B39, 1871 (1989)]. It has been found that the InAs/CdSe interface is a type-II heterojunction with the bottom of conduction band of InAs is by ~60 meV higher than that of CdSe, whereas the InAs/$Cd_{0.85}Mg_{0.15}Se$ interface is a type-I heterojunction with the bottom of conduction band of the CdMgSe alloy higher than that of InAs by ~160meV (as follows from CdMgSe/CdSe band offset study) and a large valence band offset DE_V~1.6 eV (Fig. 8).

The CdMgSe energy gap versus composition dependence has been determined using PL and EPMA data (Fig. 7). The optical bowing parameter *?* = 0.2 eV as well as the zinc-blend MgSe band-gap energy $E_g^{\Gamma}(MgSe)$ = 4.05eV have also been determined. A DE_V/DE_g ratio, where DE_V is the valence band offset, is another characteristic parameter of the CdSe/CdMgSe heterostructure system, which we have estimated, combining the experimental DE_V value for a MgSe/$Cd_{0.56}Zn_{0.44}Se$ structure [*Wang et al., Appl.Phys.Lett.* ***64****, 3455 (1994)*] with the well known ratio DE_V/DE_g=0.25 for the ZnCdSe/CdSe system. As a result, DE_V/DE_g is ~0.3 for CdSe/$Cd_{1-x}Mg_xSe$, i.e. in other words DE_V=0.66*x* (eV). Calculations of optical transition energies

in CdSe/CdMgSe quantum wells (QWs) in the effective mass approximation, using the above determined parameters and taking account of strain influence

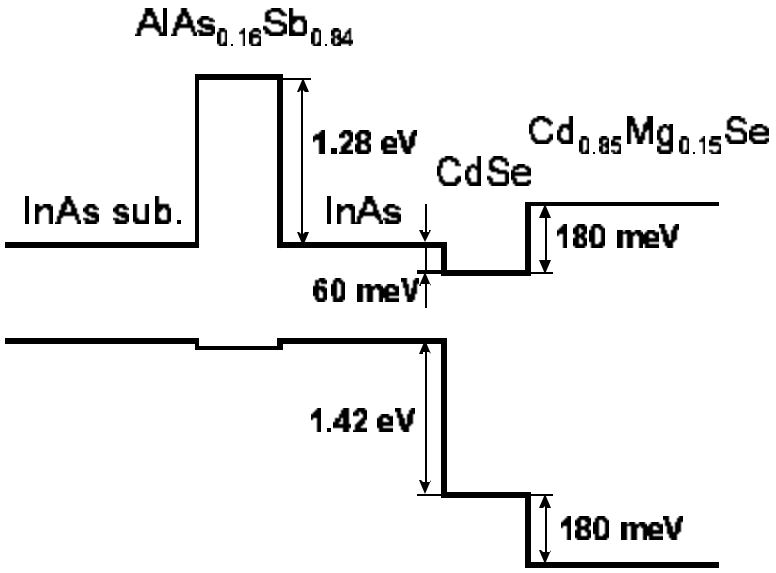

Fig. 8. Schematic band diagram of a hypothetical InAs/AlSbAs/InAs/CdSe/CdMgSe heterostructure.

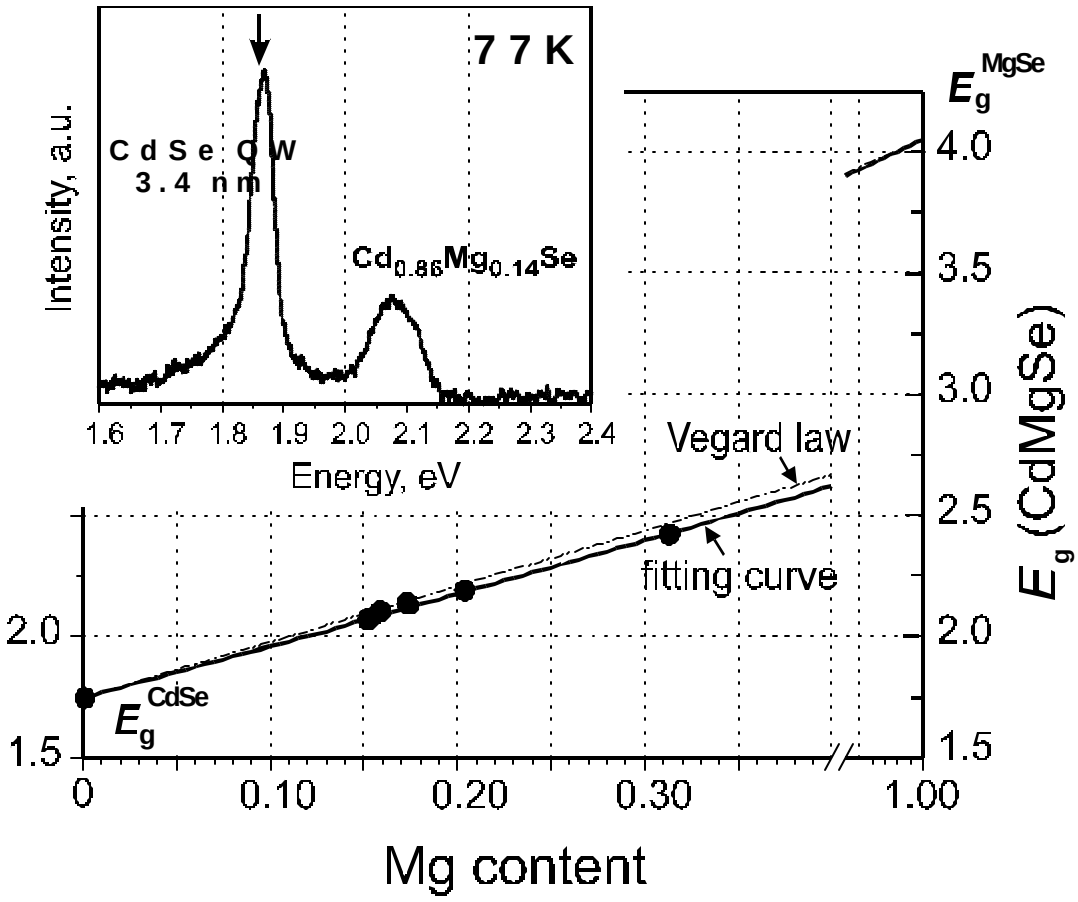

Fig. 9. E_g versus x dependence for the $Cd_{1-x}Mg_xSe$ system. Circles are the experimental data. Solid curve is a $E_g(x)$ theoretical estimation using optical bowing parameter C= 0.2 eV. Dashed line follows the Vegard's law. Inset shows low-temperature PL spectrum of the 3.4 nm-CdSe/CdMgSe QW structure, with the arrow denoting the calculated energy of the QW PL peak energy.

on the band offsets at the CdMgSe/CdSe interface, yields the values consistent well with experimental PL data of the QW structures (compare the arrow position in the inset of Fig. 9 with the QW PL peak energy).

The preliminary electroluminescence (EL) studies of the hybrid structures with and without a thin CdSe layer at the InAs/II-VI interface in between CdMgSe and InAs has demonstrated good agreement with the above band line-up at the (Cd,Mg)Se/InAs interface. Additionally, we have performed Hall measurements on the similar hybrid structures with a 20 nm-InAs QW confined on the one side by a AlSb barrier and on the other side by (Cd,Mg)Se layer grown on semi-insulating GaAs substrates with GaSb buffer layer. One sample with the InAs/CdSe interface exhibits electron in-plane mobilities as low as μ_e=800 cm^2/Vs and μ_e=500 cm^2/Vs at 300 and 77K, respectively. These values fit well the mobility of the bulk hexagonal n-type CdSe, which agrees in general with the suggested absence of the 2DEG channel in InAs due to the electron accumulation in the CdSe QW. Contrary to that, another sample with the InAs/$Cd_{0.85}Mg_{0.15}Se$ interface demonstrates much larger mobilities, μ_e=2700 cm^2/Vs and μ_e=2200 cm^2/Vs at 300 and 77K, respectively. These values can hardly be ascribed to CdSe, indicating most probably the confinement of electrons on the InAs side of the InAs/CdMgSe interface. The observed InAs 2DEG mobility values are much smaller than those usually obtained in the complete AlGaSb/InAs/AlGaSb QWs (in excess of 150,000 cm^2/Vs at 77K), which can be explained by defect generation at the AlGaSb/InAs interface due to strain relaxation in the InAs/Cd(Mg)Se upper part of the hybrid structure, nearly lattice-matched to InAs, with respect to the GaSb buffer layer. The extremely high defect density generated in the QW is believed to cause the observed reduction of the mobilities with the temperature decrease. Thus, these data are also in good qualitative agreement with the theoretical estimate.

2.3. Characterization of the hybrid structures

2.3.1. Structural characterization

The hybrid structures were studied by cross-sectional scanning electron microscopy (SEM). The typical SEM image of the hybrid laser structure, derived using secondary electron

mode, is presented in Fig. 10 and demonstrates the high quality and planarity the structure layers as well as reproducibility of the layer thicknesses.

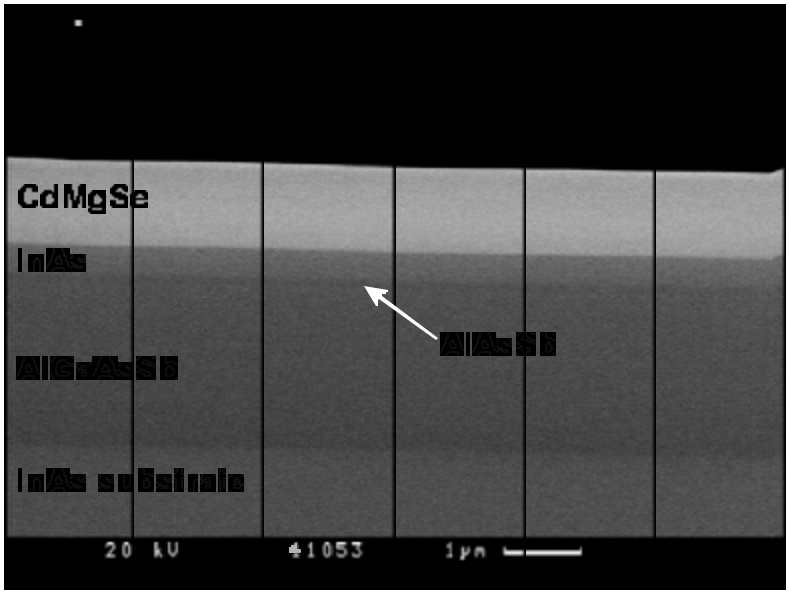

Fig. 10. Cross-sectional SEM image of the hybrid *p-n* InAs:Be/$Al_{0.48}Ga_{0.52}Sb_{0.88}As_{0.12}$:Be/InAs/ $Cd_{0.9}Mg_{0.1}Se$:Cl laser structure (#41053).

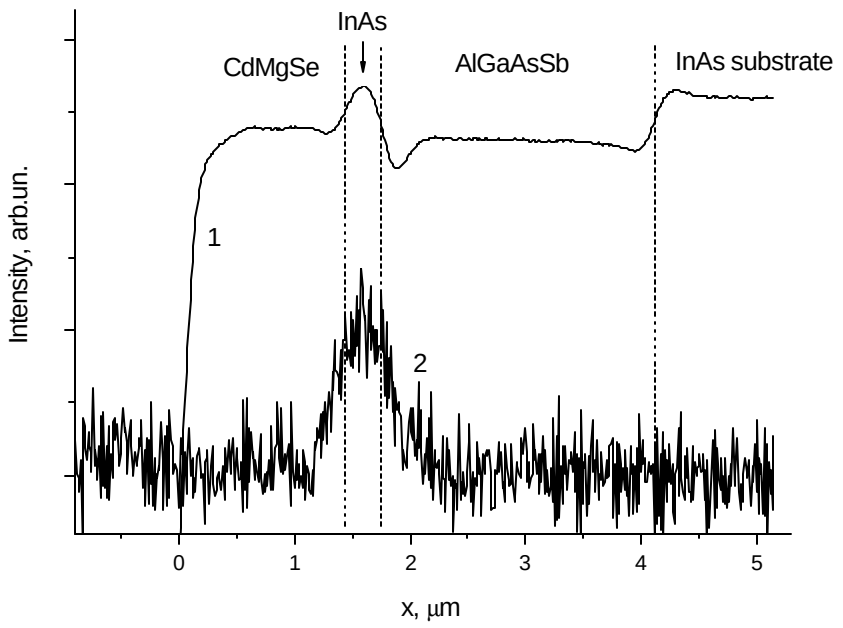

Fig. 11. The BSE (1) and EBIC (2) line profiles measured under electron beam scanning across the cleavage plane of the hybrid *p-n* InAs:Be/$Al_{0.48}Ga_{0.52}Sb_{0.9}As_{0.1}$:Be/InAs/$Cd_{0.9}Mg_{0.1}$Se:Cl laser structure (#41051).

To control the p-n junction location in the diode structures, some of them were investigated by SEM with the use of electron beam induced current (EBIC) mode. Fig. 11 shows the line profiles of the back-scattered electron (BSE) and EBIC signals measured under electron beam scanning across the cleavage plane of the hybrid *p-n* InAs:Be/$Al_{0.48}Ga_{0.52}Sb_{0.9}As_{0.1}$:Be/InAs/$Cd_{0.9}Mg_{0.1}$Se:Cl laser structure (#41051). The BSE mode is used for the determination of heterojunction positions, whereas the EBIC peak maximum points to the position of the center of a space charge region (SCR). In this structure AlGaAsSb layer was doped by Be and InAs active layer was intentionally undoped. The Hall measurements performed in the structure containing 0.6 μm-thick InAs undoped layer grown on a high resistivity InAs substrate (n~ 10^{15} cm^{-3}), gives electron concentration as low as n= $3 \cdot 10^{16}$ cm^{-3}. Thus, SCR is supposed to be mainly located in the InAs active layer. This is confirmed by the EBIC data, as the EBIC peak maximum is positioned near the centre of the active layer (Fig. 11).

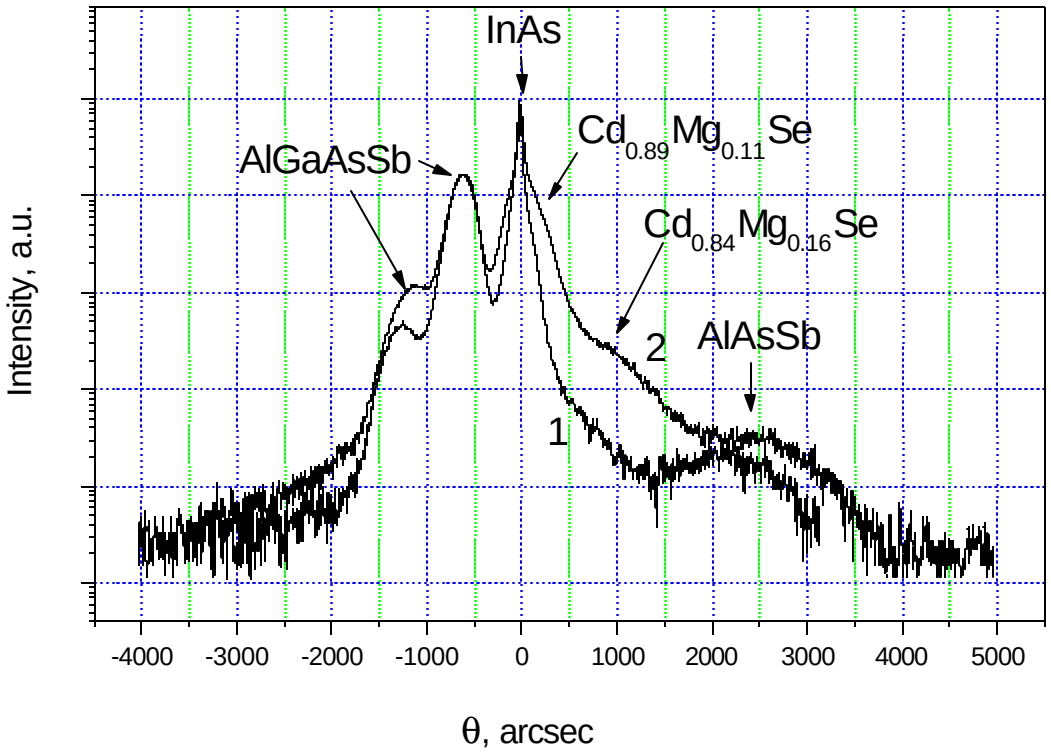

Fig. 12 X-ray diffraction Θ–2Θ rocking curves of the III-V part (1) and the whole hybrid laser structure #41052 (2).

The structural properties of the hybrid heterostructures have been studied in detail by XRD. Since the structures are rather complicated and consist of many layers, we have measured XRD rocking curves of both the finished hybrid structures and in the III-V parts as grown. The results of such measurements for the one of the hybrid laser structures (# 41052) are shown in Fig. 11. One can see four peaks in the XRD spectrum of the III-V part (curve 1). Two of them at ~ - 600 and ~ -1200 arcsec correspond to the thick AlGaAsSb layer with some gradient composition due to instability of Sb vapor pressure during the ~3 hours growth. The third peak at 0 arcsec fits well a substrate and InAs buffer layer. At last, the fourth weak and wide peak at ~ 2300 arcsec represents thin $AlAs_ySb_{1-y}$ barrier at the AlGaSbAs/InAs interface with As content of y~ 0.23, derived from the peak position, assuming it is fully strained. The comparison of the XRD curves in Fig. 12 evidences that II-VI growth does not degrade the structural quality of the structure as a whole. However, small modification of the spectra in the region of AlGaAsSb-related peaks is supposed to result from superposition of these peaks with that from strained

CdSe contact layer. Actually, the position of CdSe-related peak calculated for the non-relaxed layer is about - 850 arcsec. The nearest shoulder on the right hand of the InAs-related peak corresponds to the thick II-VI cladding layer nearly lattice-

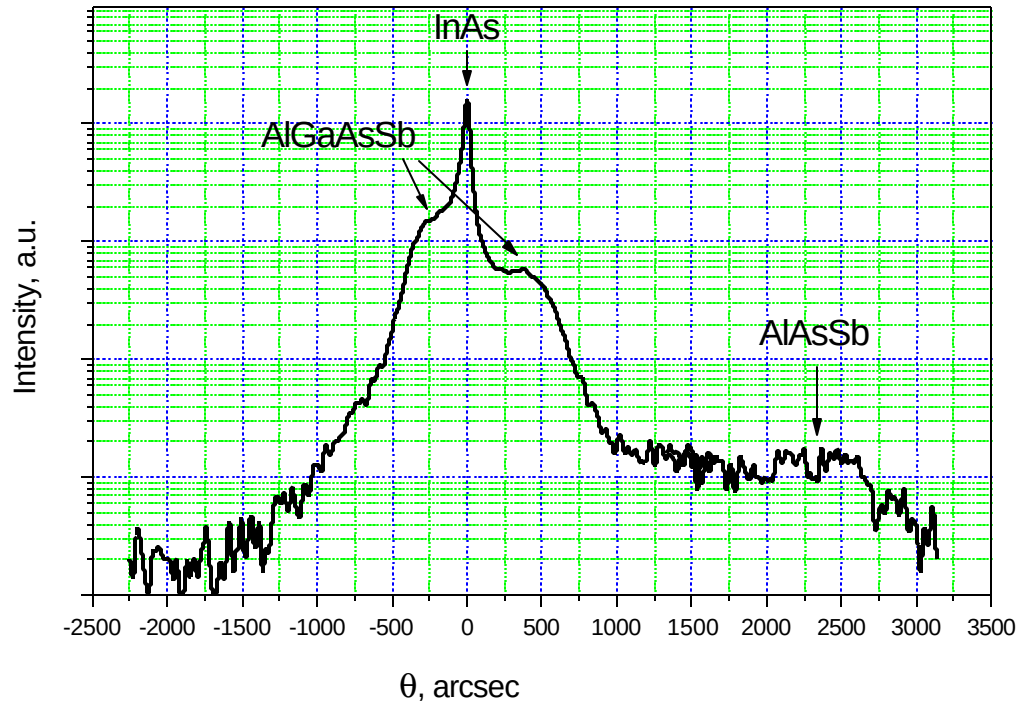

Fig. 13 X-ray diffraction Θ–2Θ rocking curve of the III-V part of the hybrid laser structure #41070.

matched to InAs. The estimation of its composition from the XRD spectrum gives $Cd_{0.89}Mg_{0.11}Se$. Another small shoulder at ~ 1100 arcsec is due to thin 30 nm–$Cd_{0.84}Mg_{0.16}Se$ grown direct on InAs active layer to improve the electron confinement from the II-VI side. Fig. 13 shows XRD rocking curve for the III-V part of the hybrid laser structure (# 41070) that demonstrates stimulated emission. In this structure AlGaAsSb layer is nearly lattice-matched to InAs, as clearly seen in Fig. 13. The II-VI growth features were the same as in structure #41052.

2.3.2. Photoluminesence studies

In order to estimate the quality of the layers and III-V/II-VI interfaces, photoluminescence (PL) studies were performed over a wide spectral region. We used single-grating monochromators and different excitation sources for different spectral regions. An InGaAs cw laser diode emitting at 950 nm was used to excite PL in the III-V part of the structure, responsible for emission in the infra-red (IR) spectral region, while a 325 nm line of a

cw He-Cd laser was used to excite PL from the CdSe and CdMgSe layers. The hybrid structures show generally intense PL in both infrared and visible spectral regions. Figure 14

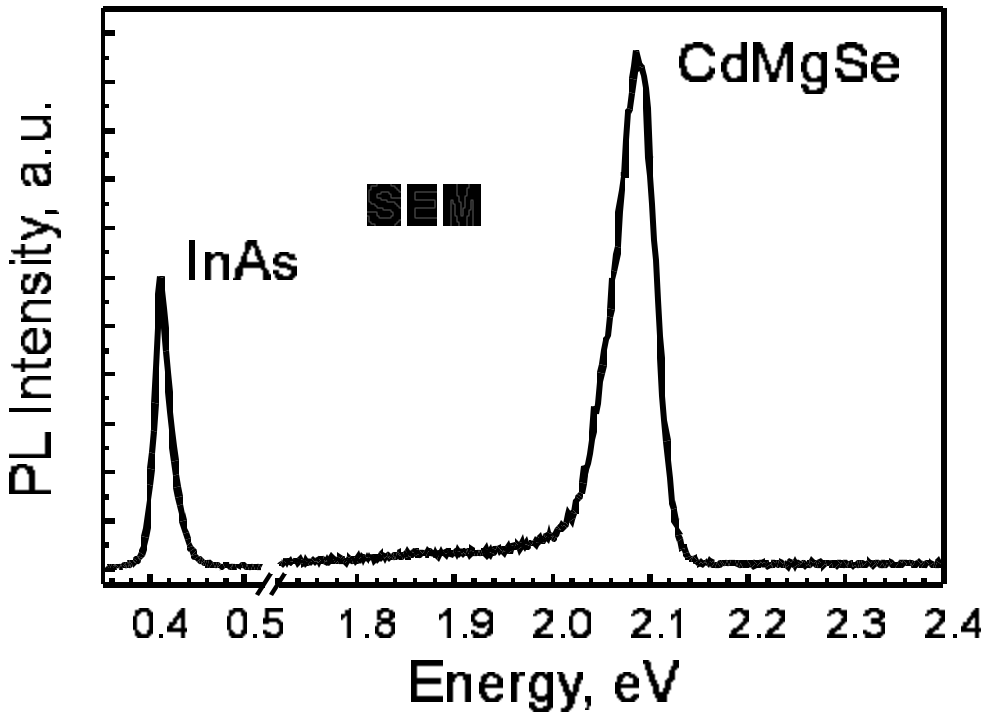

Fig. 14 PL spectra at 80K of the hybrid *p*-InAs/*p*-AlGaAsSb/InAs/*n*-CdMgSe/*n*-CdSe laser structure.

demonstrates PL spectra measured at 80K in the hybrid *p*-InAs/*p*-AlGaAsSb/InAs/*n*-CdMgSe/*n*-CdSe laser structure. Two relatively narrow peaks are visible at 0.41 eV and 2.08 eV, which are attributed to the near-band-edge PL in InAs and $Cd_{0.86}Mg_{0.14}Se$ layers, respectively. We have also studied the IR region of PL spectra in dependence of pumping power for two hybrid laser structures differing from each other by *p*-*n* junction location. In the

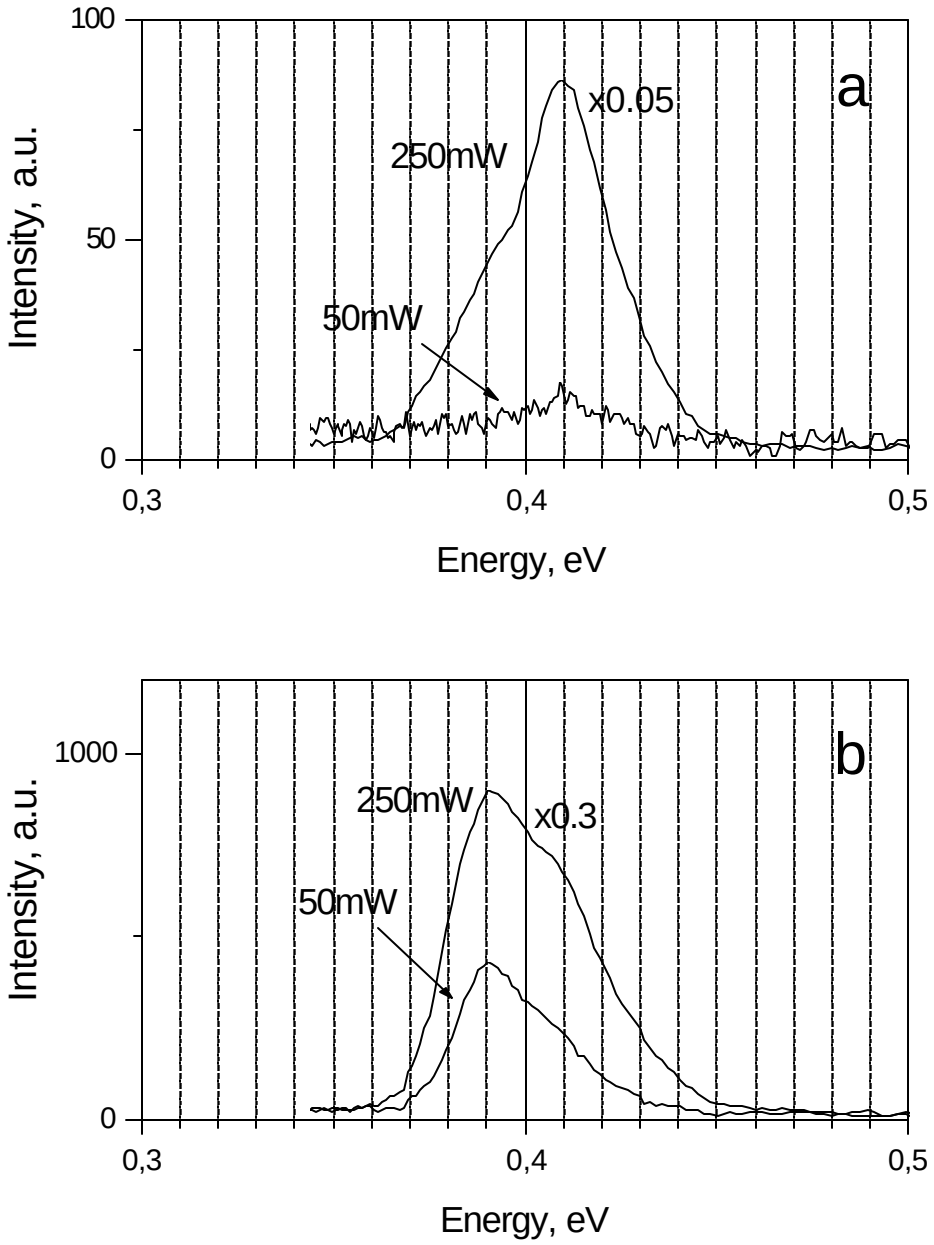

Fig. 15 PL spectra at 80K and different excitation powers of the hybrid laser structures with p-n junction inside the InAs active region (a) and at the AlAsSb/InAs interface (b).

structure #41052, we doped by Be the buffer InAs, AlGaAsSb layer and first 60 nm of the InAs active layer, whereas in structure #41051 all of the active layer was intentionally undoped. The PL spectra of the structures measured at different pumping powers are shown in Fig. 15a and b, respectively. At rather low pumping power the intensity of PL peak of structure #41052 is lower by about order of magnitude than that of structure #41051. But with power increasing the former demonstrate drastic rising and the difference becomes negligible. Such PL spectra behavior

evidences the presence of strong built-in electric field in the active region of #41052 that separates non-equilibrium carriers and prevents their radiative recombination of them.

2.4. Post-growth treatment of hybrid lasers heterostructure

Starting with this, a chemical etchant was studied and established in order to use one for whole heterostructure which consisted of three main different parts: InAs-rich and GaSb-rich solid solutions forming A^3B^5 region and properly A^2B^6 region. We have made progress in this direction playing with the content and concentration of the etchant. Moreover, we have developed special procedure of wet chemical etching under external drive current that allows controlling tangential and longitudinal components of the etching rate.

We have produced mesa-stripe structures with double-channel profile and a stripe width 80 μm. The width of contact stripe area was 50 μm. Consecutive three-layer sputtering of Cr, Au+Zn alloy and Au cover, respectively, formed ohmic contacts to p-InAs side. For n-CdMgSe compounds metallic In was used as good ohmic contact. Laser structure chips were mounted on a cupper heatsink and bound by Au wire. To suppressed surface leakages there are three types of oxide covering under study starting from conventional oxidation of heterostructure surface and $Si0_2$ covering and up to polyamide compounds and nitride content compounds as well.

I-V characteristics were measured for three types of heterostructures n-InAs/P-AlGaAsSb, p-InAs/n-CdMgSe and laser structure P-AlGaAsSb/n-InAs/n-CdMgSe. Diode like behaviour of I-V characteristics was observed for n-InAs/P-AlGaAsSb with thick layer (h~0.7 μm) of AlGaAsSb quaternary solid solution while the ohmic behaviour was found for n-InAs/n-CdMgSe. It can be concluded that basic part of voltage drop is concentrated near III-V heterointerface. The I-V characteristics for p-InAs/p-AlGaAsSb/n-InAs/n-CdMgSe laser structure at 77 K and 300 K are presented in Fig.16. As clear shown in the figure that direct curve cut-off at room temperature can be associated with narrow-gap active layer of the laser (U_{300}~0.25 V) while with temperature decreasing towards 77 K the cut-off value increases in the order of three (U_{77}~0.8 V). The observed inhomogeneous on the I-V direct curve at 77 K indicates also that there are additional drive current flows involving the wide-gap of the laser hetetrostructure.

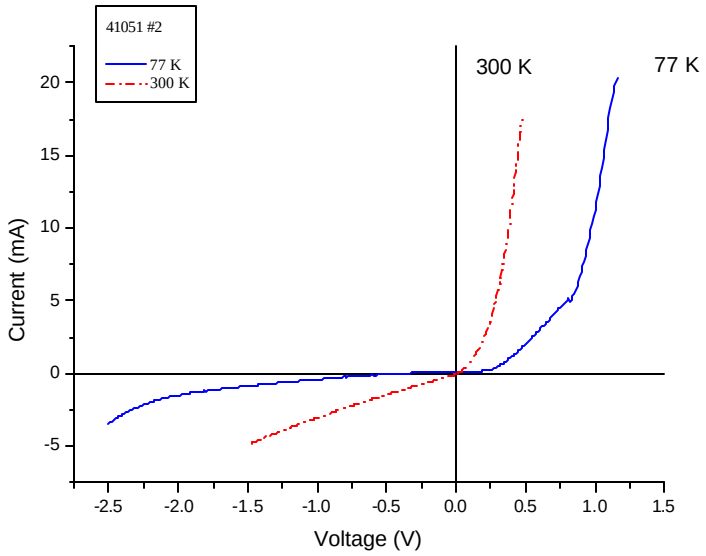

Fig.16. Dependence of drive current on the external bias at 77? and 300 ?

2.5. Electroluminesence and lasing study

Electroluminescence studies of spontaneous emission from the III-V/II-VI hybrid laser structures have been performed on the mesa diodes of 300 μm diameter with a 50 μm round contact, fabricated using a standard photolithography and deep wet chemical etching.

Comparative EL studies of the hybrid laser structures with and without a 10nm-CdSe layer grown between InAs and CdMgSe layers have been carried out (samples A - #1864 and B - #1865, respectively, in Fig. 17). Sample A shows the bright InAs related EL peak shifting to higher energies with increasing the pumping current. In contrast, sample B exhibits EL peak position shifted towards low energy of 30 meV in comparison of the EL peak from InAs. Moreover, one can observe a dramatic decrease in the EL intensity of sample B. Taking into account these results, we

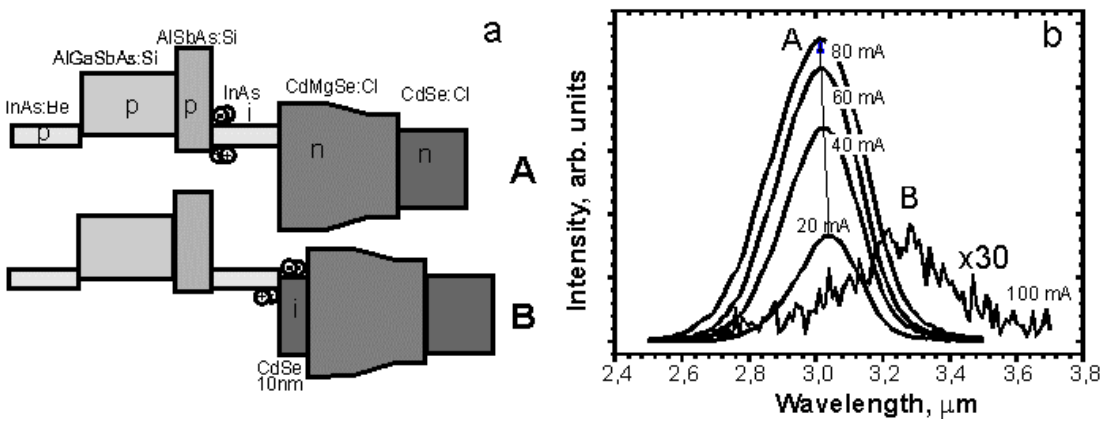

Fig. 17. Schematic band diagram (a) and electroluminescence spectra at 77 K (b) of the hybrid structures with (B, #1865) and without (A, #1864) CdSe QW adjusted to InAs.

believe that in the latter case EL is defined by electron-hole recombination at the type II InAs/CdSe heterojunction containing large enough density of non-radiative recombination defects, while in the former structures EL originates at the high quality AlAsSb/InAs interface.

Luminescent properties of hybrid GaAlAsSb/InAs/CdMgSe structure based on the combination of A^3B^5-A^2B^6 solid solutions were studied in large drive current range under pulsed regime and quasi-steady state conditions at liquid nitrogen and room temperature.

Typical laser structure was grown on p^+-InAs substrate and contained III-V part consisting of buffer InAs:Be 50 nm-layer, thick $Al_{0.5}Ga_{0.5}As_{0.12}Sb_{0.88}$:Be 2.3 μm-layer with small gradient layer at the top of it and confined by 20 nm-$AlAs_{0.2}Sb_{0.8}$:Be layer, and undoped n^0-InAs layer as thick as 0.5 μm. The II-VI part of the structure consisted of n-CdMgSe:Cl 1 μm-layer with various content of Mg from 15% at the InAs/CdMgSe heteroboundary to 10%, that corresponds to lattice-matching with InAs substrate. A heavy doped CdSe:Cl layer was used as cap layer as thick as 100 nm.

The samples for the study were manufactured as stripe-etched laser structures mounted on the copper heatsink. The cavity length was as long as L=500 μm and stripe width as wide as d=30 μm was formed by etched double-channel profile. Intense spontaneous luminescence and coherent emission was obtained for the first time in the hybrid GaAlAsSb/InAs/CdMgSe heterostructure.

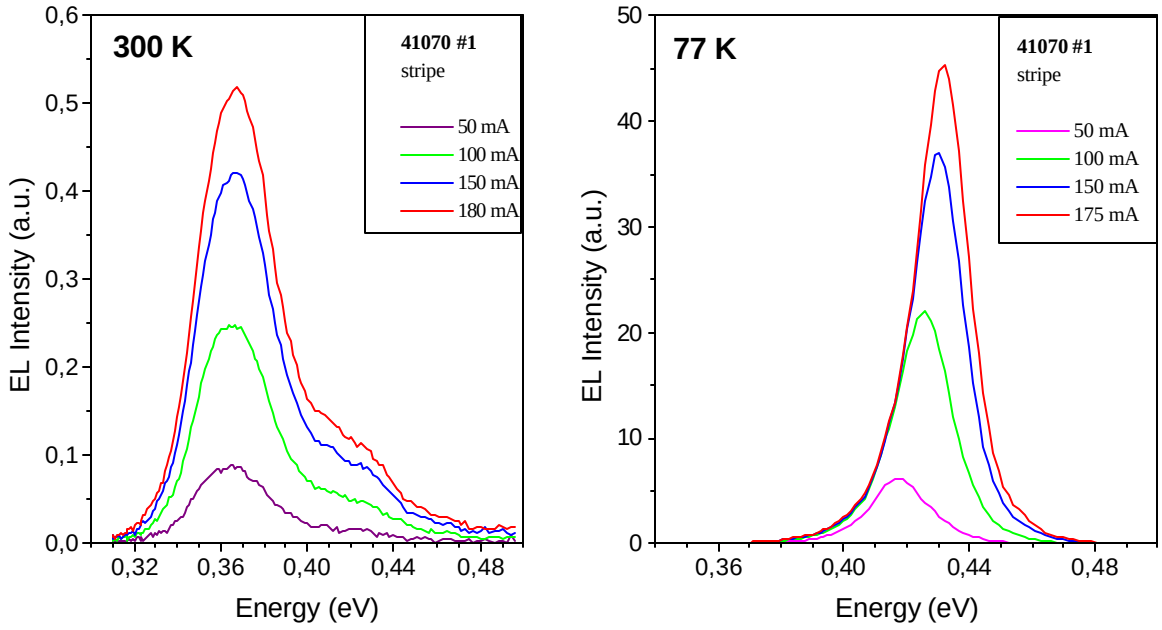

Fig.18. EL spectra for the hybrid heterostructure at 80 K (a) and 300 K (b) under different drive current

Electroluminescence (EL) was observed at large temperature range from 77 K to 300 K under quasi steady-state conditions. Long-duration pulses (τ=1ms) of drive current with repetition rate of f=500 Hz were varied in the range up to 200 mA. The room temperature EL was obtained in a spectral range 0.3-0.5 eV (Fig. 18). EL spectra contained single pronounced emission band $h\nu_1$=0.374 eV. The second emission band $h\nu_2$=0.423 eV as additional shoulder of the main band at high-energy edge of the spectrum was found under high-level injection. A small shift (2-3 meV) of peak spectral position towards high energy with drive current increasing was observed while the "blue" shift for the emission band maximum at 77 K was spreading of 18 meV from 0.418 eV to 0.436 eV (Fig. 19a). It should be to note that the luminescence at low temperature was starting with photon energy $h\nu_{77}$=0.418 eV. EL spectra at 77 K contained single pronounced emission band as well and the asymmetric shape of the emission band with sharp high-energy edge but without any additional peaks that can be appear at high current injection level. With temperature decreasing from 300 K to 77 K the spontaneous emission intensity increased in the order of 2. It should be to notice that the emission intensity demonstrated linear dependence on drive current (Fig. 19b).

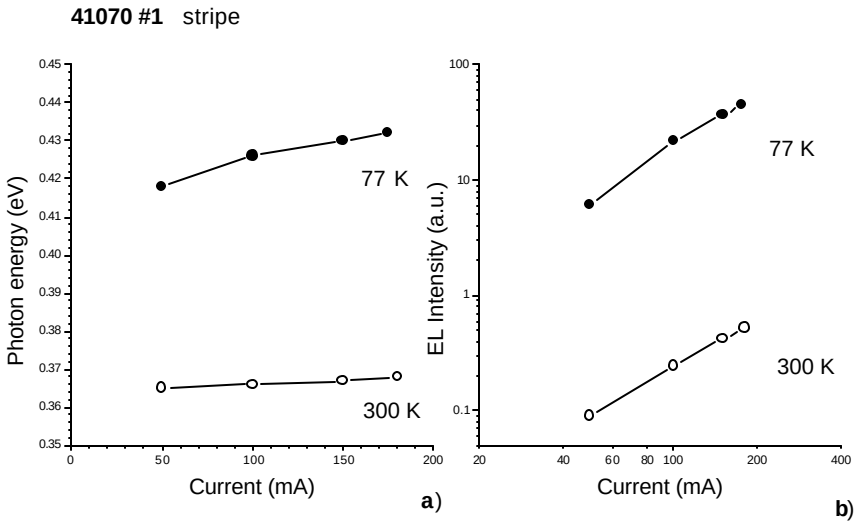

Fig.19. Dependence of spectral position of EL peak (a) and EL intensity on drive current.

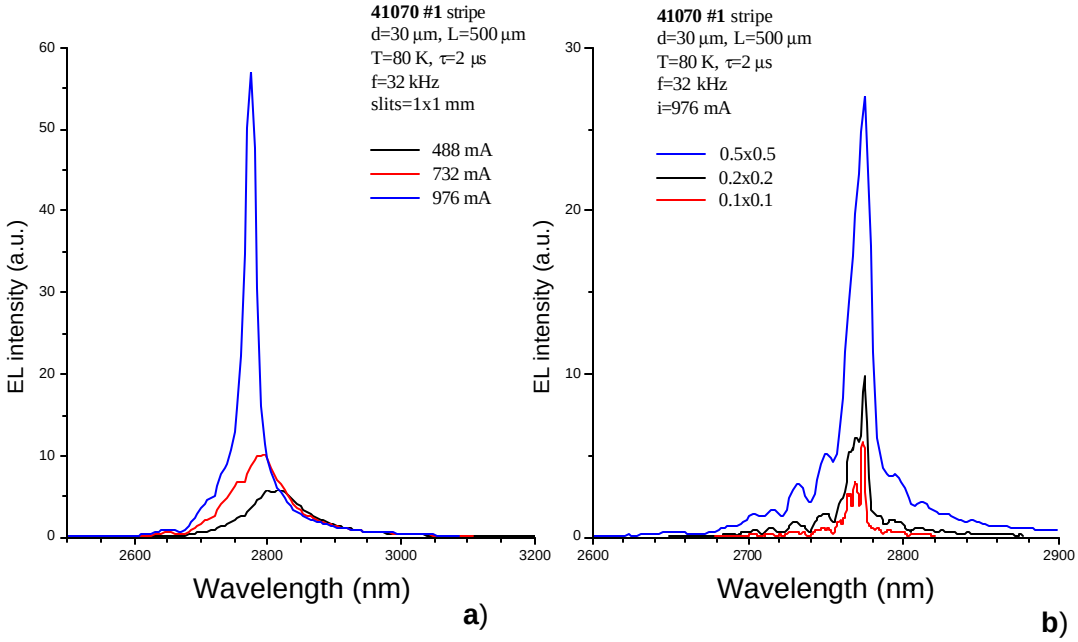

Fig.20. Electroluminescene at the lasing threshold

Coherent emission was achieved at 77 K under pulsed regime. Short-duration pulses of the drive current in the duration range from 2 µs to 125 ns were applied on the structure under repetition rate of 32 kHz. With drive current increasing the “blue” shift of the main emission

band maximum was observed still from 0.436 eV to 0.442 eV (Fig. 20a). As was shown in Fig. 20b the slits width decreasing allows us to draw out separated modes from the spectrum and the main lasing band was defined through the background.

A threshold current value was evaluated as I_{th}=680 mA for 500 ns duration pulses and I_{th}=488 mA for 2 μs duration. That value corresponded to the pulse threshold current density as low as j_{th}=3-4 kA/cm^2. Single-mode lasing was peaked at λ=2.775 μm that corresponds to photon energy at maximum of the emission band $h\nu_{lasing}$=0.446 eV. An average inter-mode distance was about of 50 Å while the half-width of main lasing peak did not exceed 30 Å.

As mentioned above, the pulse threshold current density j_{th}=4 kA/cm^2 was computed for 500 ns pulse duration. The increasing drive current the increasing output power (Fig. 21). However, the threshold current exceeded in two times leads to the increasing of heterostructure internal warming-up that results in dramatic reducing of lasing intensity.

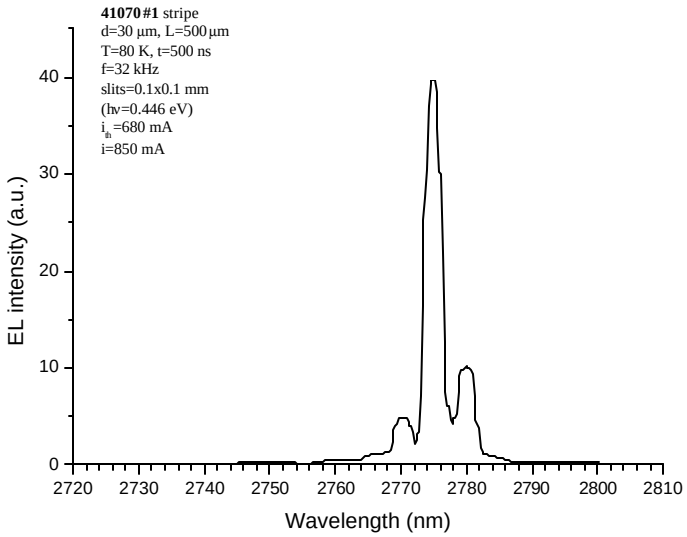

Fig. 21. Lasing spectrum for the hybrid heterostructure in pulsed mode at 80 K

A temperature dependence of threshold current for hybrid laser structure in pulsed mode is presented in Fig. 22. The operating temperature range has been confined by 100 K for this pilot version of infrared laser, which, however, inhibits intense spontaneous luminescence at room temperature. This fact indicates there are some different radiative recombination mechanisms that can realized at low and high temperature separately. It forces to pay more intent attention during next laser structures development.

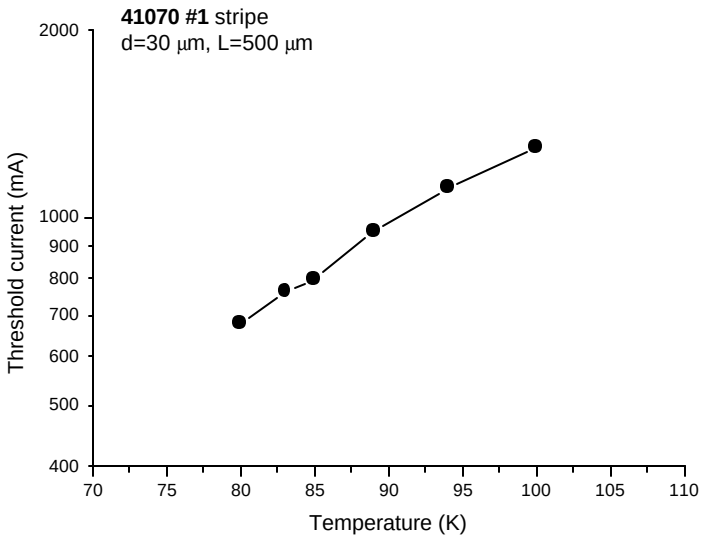

Fig.22. Temperature dependence of threshold current for the hybrid heterostructure in pulsed mode (f=32 kHz, τ=500 ns)

2.6. Fabrication and study of MOVPE grown InAsSbP/InAsSb/InSbP asymmetric laser structure with high phosphorus content.

2.6.1. Growing of InAsSbP/InAsSb/InSbP heterostructure with high phosphorus content by MOVPE.

InAsSbP/InAsSb/InPSb double heterostructure (DH) was grown in a horizontal flow MOVPE reactor under atmospheric pressure. Epilayers were grown on InAs substrate placed on molybdenum susceptor with bottom heating by resistance heater. The total flow of hydrogen through the reactor was 18 l/min. The precursors were trimethylindium (TMIn), trimethylantimony (TMSb), diethylzinc (DEZn), phosphine (PH_3) and arsine (AsH_3) that were H_2 diluted to 20%. TMIn, TMSb, and DeZn bubblers were kept at 28^0C, -6^0C and 5 ^{0}C, respectively, for all the experiments. InAs substrates used for the growth were doped with sulphur or zinc to carriers concentration of n ~ $2x10^{18}$ cm^{-3} and p ~ $5x10^{18}$ cm^{-3}, respectively. The n-type substrate was etched in HCL:H_2O:CrO_3 mixture prior to growth while p-type substrate was epiready.

Lattice mismatch between the substrate and the epitaxial layers was determined by double crystal XRD method. The solid phase composition of the layers was measured EPMA. SIMS was employed for measuring the level of commonly occurring impurities. Optical properties of

InAsSb layers were studied by photoluminescence (PL) method at T=77 K. The emission was recorded using a liquid N_2-cooled InSb photoresistor and a lock-in amplifier. The IKM-1 monochromator was used as a dispersive element. GaAs diode laser was used as exciting source (wavelength λ=0.8 μm, output power in pulse mode 10 W, τ=5 μs, and f=500 Hz).

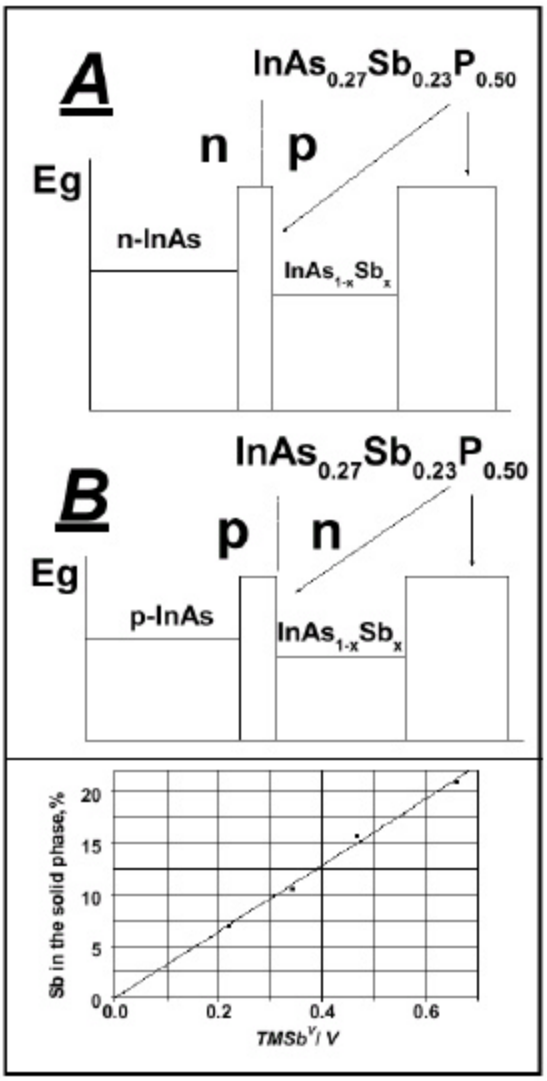

Fig. 23. Two types of the laser structures. Inset: the solid antimony deposits on the growing surface

Growth temperature for $InAs_{0.27}Sb_{0.23}P_{0.50}$ was 520^0C. The H_2 flow through TMIn and TMSb bubblers were 600 and 20 ml/min respectively. The AsH_3 and PH_3 flows were 2 and 80 ml/min, respectively. We have achieved p ~10^{18} cm^{-3} using H_2 flow of 25 ml/min through DEZn bubbler. The Zn doping levels were estimated by PL measurement of p-type InAs layers and from current-voltage characteristics for the fabricated diodes. The lattice mismatch between $InAs_{0.27}Sb_{0.23}P_{0.50}$ layer and InAs substrate $\Delta a/a$ was less than $6*10^{-4}$.

InAsSb layers were grown in the temperature range 575-610 ^{0}C. Vapor pressures of 2.97 mmHg for TMIn (25 ^{0}C), of 22.43 mmHg for TMSb (-6 ^{O}C), of 5.0 mmHg (5^{0}C) for DEZn are used for calculation of the V/III and TMSb/(TMSb+AsH_3) ratios. The best growth conditions for InAs were found at V/III ratio of 40 and nucleation temperature of 610 ^{0}C at a growth rate of 0.4 μm/h. 77 K PL spectra exhibited full width at a half maximum (FWHM) of the band edge luminescence as small as of 10 meV with the peak position at 408 meV. Using SIMS method we established that the concentration of background impurity atoms such as carbon and oxygen in these layers is below then the sensitivity of our measurement equipment (~5x10^{15} cm^{-3}). For InAsSb growth the temperature was lowered to 575 ^{0}C. The Sb content in solid phase versus TMSb/(TMSb+AsH_3) gas phase ratio is shown at the inset in Fig. 23.

2.6.2. Post-growth technology of LED's and laser structures.

The LED's were fabricated by the standard photolithography. The dot contact on the top of the chip was 100 μm in diameter. The contacts are formed by the vacuum evaporation of gold and tellurium onto an n-type layer or of gold and zinc onto a p-type layer. LED chip dimensions are 500×500 μm, 200 μm thick, and the backside of the chip being indium soldered onto the standard case. In addition, a parabolic reflector is positioned on the case in order for the angular distribution of the radiation to be narrowed down to 10-12^O.

The contact stripe width of 5 μm placed into mesa-stripe width of 30 μm. The contact stripe was made on the p-InAsSbP layer. Cavity length as long as 300 μm was made by cleaving.

2.6.3. Study of spontaneous emission and fabrication of high-efficiency LED's.

The electroluminescence (EL) was studied in the both pulse mode and quasi-steady state conditions at room temperature. The radiant power was measured using a calibrated power meter (OPHIR Ltd. firm) equipped with a 2A-SH thermocouple sensor.

Two type LEDs - "A" and "B" - were investigated. The LED structure "A" consists of an S-doped n-InAs (n~ 2x10^{18} cm^{-3}) substrate on which there were grown a 0.7 μm thick undoped $InAs_{0.27}Sb_{0.23}P_{0.50}$ cladding layer, an undoped $InAs_{1-x}Sb_x$ active region of 2.5 μm in thickness, and 2 a μm thick p-type Zn-doped $InAs_{0.27}Sb_{0.23}P_{0.50}$ cladding layer. Subsequent EBIC measurements have shown that zinc diffusion from the top cladding layer of $InAs_{0.27}Sb_{0.23}P_{0.50}$ took place, changing the conductivity of the InAsSb active layer from n- to the p-type. The p-n

junction formed in the first barrier layer $InAs_{0.27}Sb_{0.23}P_{0.50}$ was 0.5 μm apart from the n-InAs substrate.

The LED "B'' structure grown on the Zn-doped p-InAs (p ~ $5x10^{18}$ cm^{-3}) substrate involves an undoped $InAs_{1-x}Sb_x$ active layer sandwiched between Zn-doped and undoped $InAs_{0.27}Sb_{0.23}P_{0.50}$ cladding layers 0.5 μm and 2 μm in thickness, respectively. The p-n junction located at the heterointerface of the Zn-doped $InAs_{0.27}Sb_{0.23}P_{0.50}$ cladding layer and the $InAs_{1-x}Sb_x$ active layer.

The schematic band diagrams of the "A" and "B" LED heterostructures are shown in Fig. 23. The "A" and "B'' LED's chips were constructed identically with the only exception that LED's "A" are mounted with epitaxial side down, while type "B" LED's are mounted with substrate side down. Differently composed active layers (InAs, $InAs_{0.935}Sb_{0.065}$, $InAs_{0.895}Sb_{0.105}$, $InAs_{0.843}Sb_{0.157}$) were grown for LED's having various emission wavelengths. PL spectra at 77 K contain peaks for InAs at 408 meV, $InAs_{0.935}Sb_{0.065}$ at 354 meV, $InAs_{0.895}Sb_{0.105}$ at 335 meV, and for $InAs_{0.843}Sb_{0.157}$ at 326 meV. The temperature dependence of LED's EL follows the equation $Eg(T)=Eg(0)-\alpha T^2/(T+\beta)$, α=0.25 meV/K and β=80 K.

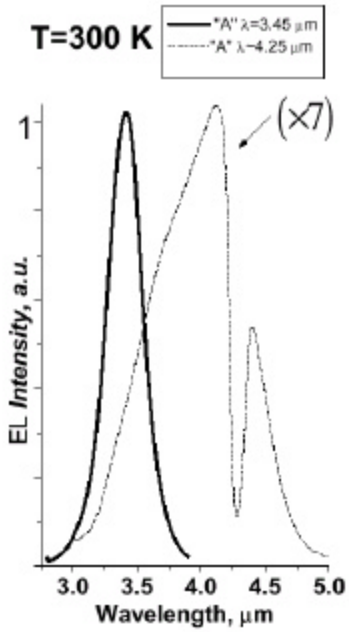

Fig. 24. Spontaneous spectra for LED's

The EL spectra of LED's "A" operating at different wavelengths at the room temperature are shown in Fig.24. The injection current was 50 mA in quasi-steady state conditions regime.

The LED's peak locations are independent of the injection current in the range 0-200 mA. EL intensity diminishes and FWHM is widened with increasing Sb content in the active layer. The growing lattice mismatch between the substrate and adjacent epitaxial structure as well as an increasing role of Auger recombination processes is the probable reason for this behaviour. For LED's with InAs active layer EL spectra peak position moves from 3.45 μm (LED's "A") to shorter wavelength 3.38 μm (LED's "B").

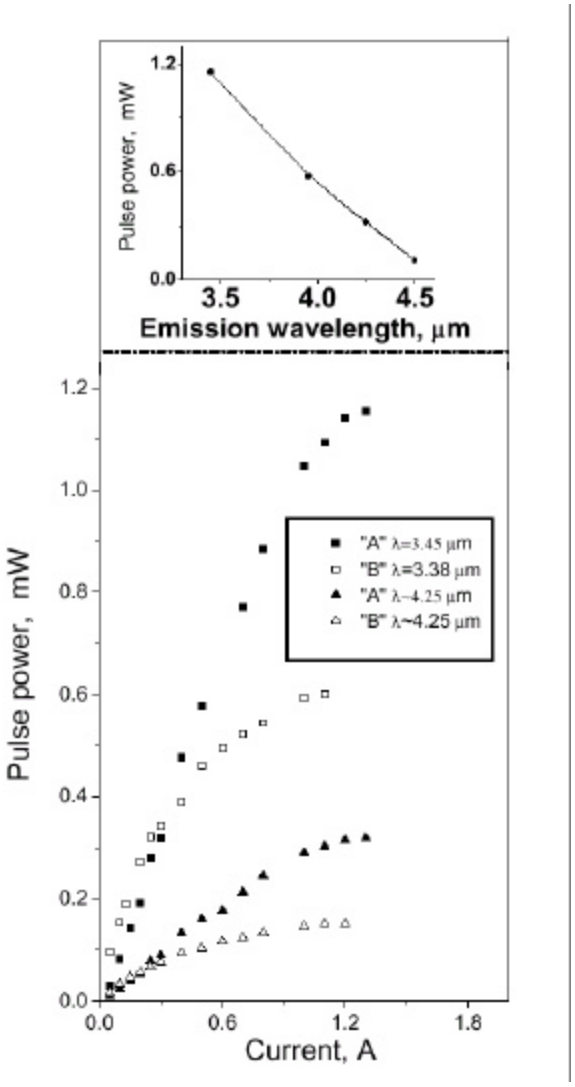

Fig. 25. Output power dependence on drive current for different LED's

This behaviour is probably caused by difference in the conductivity type of the active layer. In p-type InAs radiative recombination experiences with participation of acceptor levels located above the top of the valence band and the emission peak shifts to a slightly longer wavelength. It follows from this result that zinc diffusion from solid phase is negligible, the active area in "B'' structures has a n-type conductivity. For other wavelengths EL spectra were

nearly identical for structures “A” and “B”, and the exact peak position is difficult to determine due to strong CO_2 absorption line at 4.25 μm. Perhaps, for InAsSb active layer structures the recombination mechanism is the same as for InAs active layer, since EBIC measurements show that p-n junction position does not depend on whether InAs or InAsSb active layers have been chosen. Attempts to eliminate the Zn diffusion from the vapor phase via changes of the growth conditions appeared to be unsuccessful.

The output power of LED’s against pulsed current is shown in Fig. 25. Since “A” construction provides better heat dissipation, type “A’’ LED’s are about 100% brighter at high injection currents. But in the 0-200 mA current range, the LED’s “B’’ are more efficient than “A” due to the higher probability of radiative recombination in n-InAs than in p-InAs. The output power of LED “A” versus emission wavelength for 1.3 A pulsed current is shown at the inset in Fig. 24. Probably, non-radiative Auger recombination process $C_{Auger}*n^3$, Joule heating effect, and lattice mismatching are the limiting factors for the LED’s operation. One way toward an increasing LED’s output power is growing InGaAsSb or AlGaAsSb cladding layers with better electron confinement or employing quantum well active region in order to suppress Auger recombination and to achieve higher emission wavelength. Anyway, these diodes emit about 2 times brighter compared to commercial LPE-grown LED’s identically constructed and having the same emission wavelength.

2.6.4. Type II asymmetric GaInAsSb/InGaAsSb/InAsSbP laser heterostructure

In a framework of this project, tunnel-injection laser based on a type II GaInAsSb/InGaAsSb heterojunction with near broken-gap alignment was proposed by us and realized as alternative way. It was expected this laser structure shows good performance properties such as high operating temperature and low threshold current due to lattice-matched crystalline structure and high quality interfaces. Fig. 26 represents schematic energy band diagram of the laser structure discussed.

Type II GaInAsSb/InGaAsSb/ InAsSbP laser structures with asymmetric band offset confinements were grown by MOVPE lattice-matched to p^+-InAs (100) substrate. The undoped narrow-gap n-$InGa_{0.17}AsSb_{0.20}$ active layer (E_g=0.393 eV at 77 K) was sandwiched between doped wide-gap p-$GaIn_{0.16}As_{0.22}Sb$ (E_g=0.635eV at 77 K) and n-$InAsSb_{0.23}P_{0.50}$ (E_g=0.552 eV at 77 K) cladding layers. The thickness of InGaAsSb layer was 0.8 μm while the thickness of cladding layers was found as 2 μm. The carriers concentration of active layer was $n=2*10^{16}cm^{-3}$

and doping of the wide-gap layers was about of $p=5*10^{16}cm^{-3}$ for GaInAsSb and $n=1*10^{17}cm^{-3}$ for InAsSbP, respectively.

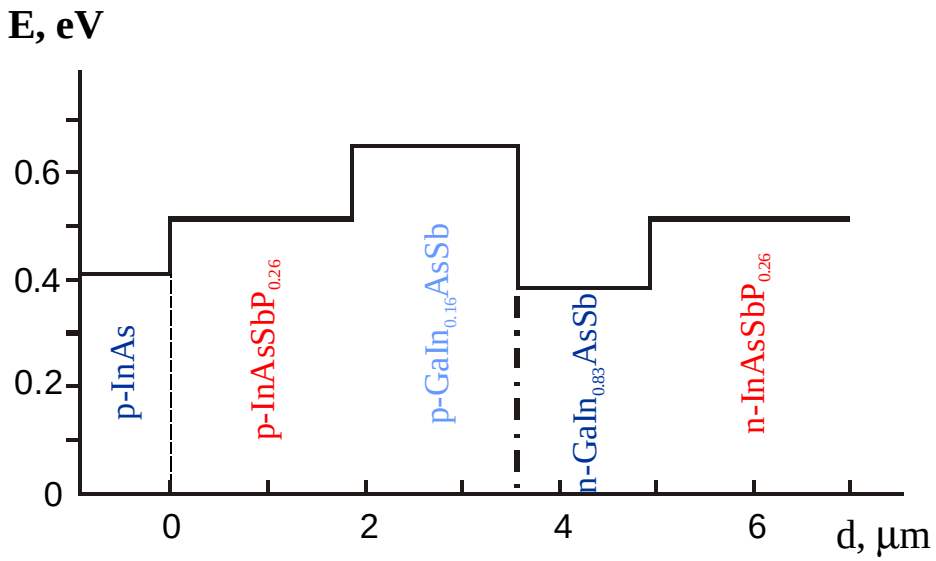

Fig.26. Schematic energy band diagram of the type II asymmetric GaInAsSb/InGaAsSb/InAsSbP laser structure

This asymmetric heterostructure allows forming the separate potential barriers at the heteroboundaries of the active region: for electrons at the InGaAsSb/GaInAsSb heterointerface (ΔE_C=0.6 eV) and for holes at the InGaAsSb/InAsSbP one (ΔE_V=0.15 eV). Besides, it manifests low barriers for the carriers injected into active region that also provides to minimize losses induced by carrier heating under injection. As was shown in Fig. 27 that the InGaAsSb/GaInAsSb interface inhibits good confinement for electrons. We also expected sufficient confinement for holes at the InGaAsSb/InAsSbP interface that results in ctimulated emission at higher operating temperatures.

Mesa-stripe laser structures were fabricated by standard photolithography with stripe width area d=110 μm and cavity length in the range L=350-750 μm. Luminescent properties of the laser structures were investigated under steady-state conditions and pulsed mode with pulse duration as τ=300 ns and repetition rate f=10 kHz.

In these structures we observed intense spontaneous and coherent emission in 3-4 μm spectral range at T=77 K. Single-mode lasing at wavelength λ=3.146 μm was achieved at 77K (Fig. 28.). A threshold current density as $j_{th}=450mA/cm^2$ was obtained for laser-stripe structure

with d=100 μm and L=750 μm. It should be noted that doublets of the emission bands as transverse and longitudinal modes of cavity length influence were observed at the spectrum.

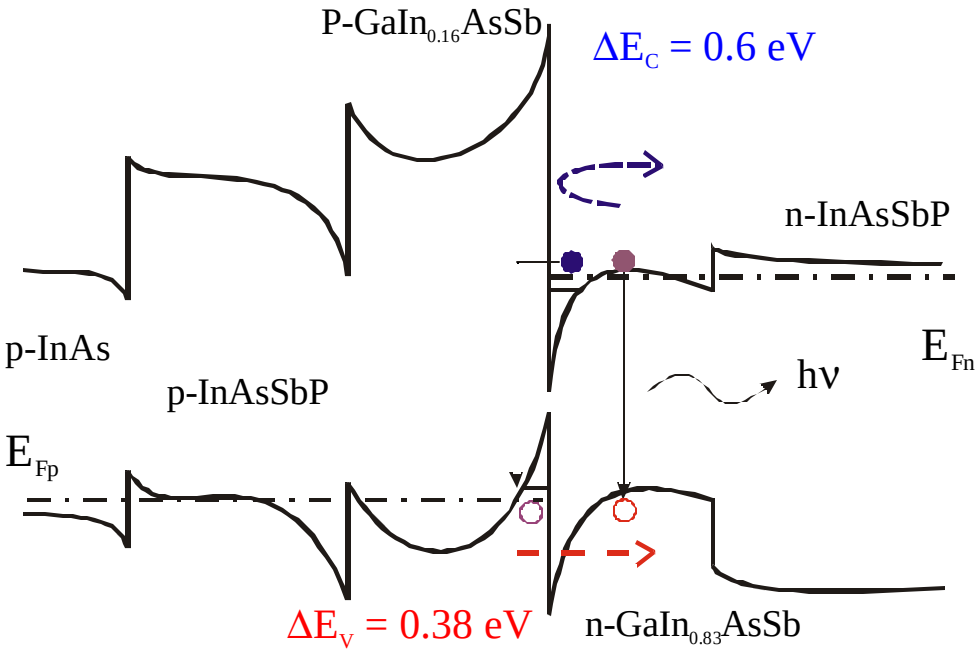

Fig.27. Schematic energy band diagram of the type II asymmetric GaInAsSb/InGaAsSb/InAsSbP laser structure under external bias

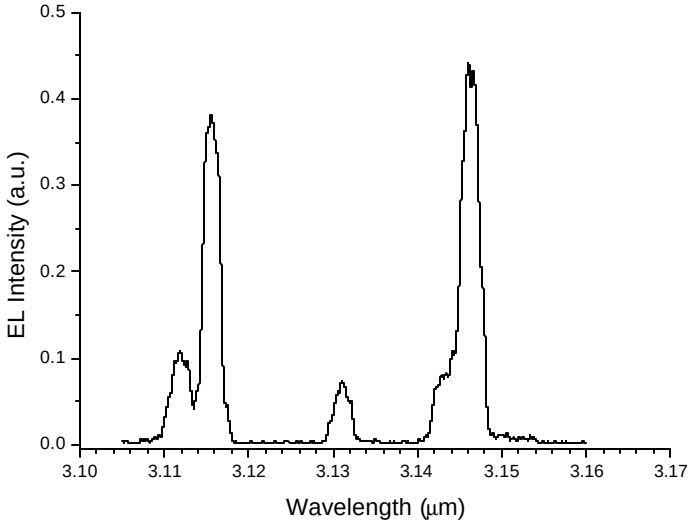

Fig.28. Lasing for the type II asymmetric GaInAsSb/InGaAsSb/InAsSbP laser structure at ? =77?

It was found that the threshold current depended only weakly on temperature at the 77-135 K range, whereas the value of the characteristics temperature (T_0) decreased from 80 K to 60 K with temperature increasing from 135 K to 160 K, and its value decreases more (up to 26 K) at high temperature range T>170 K (Fig. 29). Nevertheless, the high average T_0 value of 49 K was observed and it opens the way this laser design to create devises operating at room temperature.

Thus, the type II asymmetric GaInAsSb/InGaAsSb/InAsSbP laser structure and grown by MOVPE allows achieving an intense EL at low temperatures up to 160 K. However, it is not enough for high temperature due to poor hole confinement at the InGaAsSb/InAsSbP interface, only ΔE_V=0.15 ??, in the active region. Besides, the novel hybrid laser structure proposed above at current project inhibited strong carriers confinement at room temperature due to huge offsets at the interface for conduction and valence band simultaneously. To improve luminescent properties for narrow-gap infrared emitting structures the combination of different technology methods (for example, MOVPE plus MBE together) and advanced post-growth development are need.

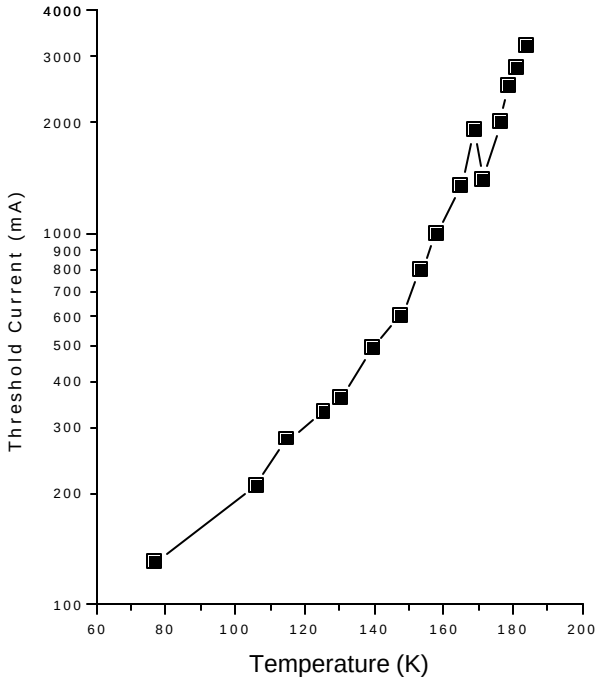

Fig.29. Temperature dependence of threshold current for the type II asymmetric GaInAsSb/InGaAsSb/InAsSbP laser structure

III. Conclusion

1. Novel hybrid III-V/II-VI laser heterostructures with strong asymmetric carrier confinement potential were proposed, fabricated and studied.
2. Two-stage MBE growth technology of III-V (AlGaAsSb/InAs) and II-VI (CdMgSe) hybrid laser structure constituents was developed to provide their high-quality structural and optical properties.
3. Different techniques of InAs surface protection (sulfur passivation and As-cap deposition) and II-VI growth initiation (low-temperature migration enhanced epitaxy of CdMgSe and thin ZnTe buffer layer) were developed to fabricate low-defect density III-V/II-VI interfaces inside laser heterostructure.
4. Theoretical and experimental studies of energy band alignment in AlGaAsSb/InAs/CdMgSe heterostructure has been performed, indicating extremely high conduction ΔE_C=1.28 eV and valence ΔE_V=1.6 eV band offset values at AlSbAs/InAs and InAs/CdMgSe interfaces, respectively. It was established that InAs/CdSe interface is of type II with potential barrier for electrons ΔE_C~0.06 eV on the InAs side, while InAs/$CdMg_{0.15}Se$ heterojunction is of type I with potential barrier for electrons ΔE_C~0.16 eV on the II-VI side.
5. Post-growth technology of laser stripe structures has been developed. Wet chemical treatment has been proposed and studied, and etching conditions of whole hybrid structure have been determined. The laser stripe in double-channel etched-out profile has been formed with Ohmic contacts made by thermal vacuum evaporation of Cr, Au and Zn mixture.
6. Intense spontaneous luminescence has been observed in the spectral range λ=3-4 μm at 300 K. Output power as high as 0.3 mW was found for round-etched mesa-diode at room temperature.
7. The most impressive result is *for the first time* observation of stimulated emission at λ=2.775 μm for the hybrid p-AlGaAsSb/n^0-InAs/n-CdMgSe laser structure at 80 K with threshold current density j_{th}=4 kA/cm^2 (Fig.1).
8. MOVPE technology of InAsSbP/InAs/InAsSbP laser structures with high phosphorous content (P>50%) has been developed. High efficiency light-emitting diodes have been fabricated and studied for the spectral range λ=3-4.5 μm with optical output power as

high as 1 mW operating at room temperature. Single-mode lasing at λ=3.04 μm for InAsSbP/InAs/InAsSbP laser heterostructure manufactured by MOVPE method has been obtained in pulsed regime at T=80 K.

IV. Outlook

Realization of lasing in the basis hybrid III-V/II-VI heterostructure with thick InAs active region opens a way to fabricate a set of novel mid-infrared optoelectronics devices (high-power lasers, light-emitting diodes and photodiodes) using advantages of both III-V and II-VI materials as well as of type I and type II heterojunctions. These structures combine large band offsets for strong electron and hole confinement with large refractive index difference for good enough optical confinement. *Optimization of optical and electronic design of different quantum well hybrid lasers, as well as the interface fabrication technology, to improve the laser parameters is the* ***main goal*** *of the future experimental and theoretical studies.*

The main tasks can be determined as follows:

- complex study and optimization of hybrid heterostructure technology;
- optimization of doping levels of separate layers in laser structure and doping profile of the whole structure;
- fabrication of MQW structures for lasing wavelength in the 3-5 μm range;
- rising of quantum efficiency and operating temperature of laser structure;
- experimental and theoretical studies of threshold current, gain, internal losses, characteristic temperature and output power in the novel hybrid laser structure.

V. References

1. P. Werle, Appl. Phys. Lett B60, 499 (1995)
2. S.R. Kurtz, R.N. Bicfield, A.A. Allerman, A.J. Howard, M.N. Crowford, M.W. Pelczynsi, Appl. Phys. Lett 68, 1332 (1996)
3. A. Rybalwski, Y. Xiao, D. Wu et al, Appl. Phys. Lett 71, 2430 (1997)
4. I. Vurgafman, J.R. Meyer, L.R. Ram-Mahan, IEEE Photonic Technol. Lett 9, 170 (1997)
5. A. Popov, V. Sherstnev, Yu. Yakovlev, Appl. Phys. Lett 68, 2790 (1996)
6. Z. Feit, D. Kosty, R.J. Woods, P. Mak, Appl. Phys. Lett 57, 2881 (1990)
7. G.G. Zegrya, A.D. Andreev, Appl. Phys. Lett 67, 2681 (1995)
8. Yu.P. Yakovlev, T.N. Danilova, A.N. Timchenko, M.P. Mikhailova, K.D. Moiseev, V. Sherstnev, G.G. Zegrya, SPIE 3001, (1997)
9. N.A. Gun‘ko, V.B. Khalfin, Z.N. Sokolova, G.G. Zegrya, J. Appl. Phys. 84, 547 (1998)
10. K.D. Moiseev, M.P. Mikhailova, O.G. Ershov, Yu.P. Yakovlev, Semicondactors, 30(6), 223 (1996)
11. K.D. Moiseev, M.P. Mikhailova, O.G. Ershov, Yu.P. Yakovlev, Tech. Phys. Lett, 23(2), 151 (1997)
12. Yu.P.Yakovlev, M.P.Mikhailova, K.D.Moiseev, A.Monakhov, V.Sherstnev, SPIE 3947, 144 (2000)
13. Final report for EOARD contract ? F61775-99-WE016, Ioffe Physico-Technical Institute, St.Peterburg, Russia, 2000
14. S. Ivanov, P. Kop‘ev, Type II (Al,Ga)Sb/InAs quantum well structures and superlattices for opto- and Microelectronics grown by Molecular beam epitaxy, Chap.4 in vol.3 “Antimonide-Related Strained-layer Heterostructures” ed. by M.O.Manasreh Gordon Breach Sci. Publ. 1997
15. R.M. Park and N.M. Salansky, Appl. Phys. Lett. 44, 249 (1984)
16. R.F.C. Farrow, J. Vac. Sci. Technol 19, 150 (1981)
17. N. Samarth, H. Luo, J.K. Furdyna, S.B. Qadri, Y.R. Lee, A.K. Ramdas, N. Otsuka, Appl. Phys. Lett. 54, 2680 (1989)
18. F. Firszt, S. Legowski, H. Meczynska, J. Szatkowski, W. Paszkowicz, M. Marczak, J.Cryst. Growth 184/185, 1053 (1998)

19. S.V. Ivanov, K.D. Moiseev, A.M. Monakhov, I.V. Sedova, V.A. Solov'ev, M.P. Mikhailova, Ya.V. Terent'ev, B.Ya. Meltzer, A.A. Toropov, Yu.P. Yakovlev, P.S. Kop'ev, Proc. of Int. Conf. "Nanostructures: Physics and Technology", St.Petersburg, 109 (2000)
20. V.A. Solov'ev, S.V. Ivanov, K.D. Moiseev, A.M. Monakhov, I.V. Sedova, M.P. Mikhailova, Ya.V. Terent'ev, B.Ya. Meltzer, A.A. Toropov, Yu.P. Yakovlev, P.S. Kop'ev, Proc. of Int. Conf. "Laser Optics – 2000", St.Petersburg (2000)

VI. List of published papers:

1. V. A. Kaygorodov, I. V. Sedova, S. V. Sorokin, O. V. Nekrutkina, T. V. Shubina, A. A. Toropov and S. V. Ivanov, "Molecular Beam Epitaxy of Low-Strained CdSe/CdMgSe Heterostructures on InAs (001) Substrates", Phys.Stat.Sol.(b) 229(1), 19 (2002)
2. S.V. Ivanov, A.A. Toropov, I.V. Sedova, V.A. Solovyev, Ya.V. Terentyev, V.A. Kaygorodov, M.G. Tkachman, P.S. Kop'ev, and L.W. Molenkamp, "MBE Growth and Luminescence Properties of Hybrid Al(Ga)Sb/InAs/Cd(Mg)Se Heterostructures, J.Cryst.Growth, 227/228, 693 (2001)
3. V.A. Solov'ev, I.V. Sedova, A.A. Toropov, Ya.V. Terent'ev, S.V. Sorokin, B.Ya. Mel'tser, S.V. Ivanov and P.S. Kop'ev, Structural, luminescence and transport properties of hybrid AlAsSb/InAs/Cd(Mg)Se heterostructures grown by molecular beam epitaxy, Semicond., 35(4), 419 (2001)
4. S.V. Ivanov, V.A. Solov'ev, K.D. Moiseev, I.V. Sedova, Ya.V. Terent'ev, A.A. Toropov, B.Ya. Mel'tser, M.P. Mikhailova, Yu.P. Yakovlev, P.S. Kop'ev, "Room-Temperature Midinfrared Electroluminescence from Asymmetric AlSbAs/InAs/CdMgSe Heterostructures Grown by Molecular Beam Epitaxy", Appl.Phys.Lett., 78(12), 1655 (2001)
5. V. A. Kaygorodov, V. S. Sorokin, I. V. Sedova, O. V. Nekrutkina, S. V. Sorokin, T. V. Shubina, A. A. Toropov and S. V. Ivanov, "Single Cd(Mg)Se Layers and CdSe/CdMgSe Heterostructures Grown by Molecular Beam Epitaxy on InAs(001) Substrates", Acta Phys.Polon. A, 100 (3), 443 (2001)

6. K.D.Moiseev, A.A.Toropov, Ya.V.Terentiev, M.P.Mikhailova, Yu.P.Yakovlev "Photoluminescence of $Ga_{(1-x)}In_xAs_ySb_{(1-y)}$ solid solutions ($0.08<x<0.22$) lattice-matched to InAs" Semicond., 34(12), 1432 (2000)
7. Yu.P. Yakovlev, S.V. Ivanov, K.D. Moiseev, A.M.Monakhov, V.A. Solovèv, I.V. Sedova, Ya.V.Terent'ev, A.A. Toropov, M.P. Mikhailova, B.Ya. Meltzer and P.S. Kop'ev "Novel hybrid III-V/II-VI mid-infrared laser structures with high asymmetric band offset confinements" Proc. SPIE Vol. 4651, p.203, 2002
8. S.S. Kizhaev, N.V. Zotova, S.S. Molchanov, B.V. Pushnyi, Yu.P. Yakovlev "Powerful InAsSbP/InAsSb light emitting diodes grown by MOVPE" IEE Proc. Optoelectr. 149, 33 (2002)
9. E.A. Grebenshchikova, N.V. Zotova, S.S. Kizaev, S.S. Molchanov, Yu.P. Yakovlev "InAs/InAsSbP light-emitting structures grown by Vapor-Phase epitaxy" Phys.Tech.Lett., 46(9), 58 (2001)

VII. List of presentations at conferences:

10. S.V. Ivanov, S. V. Sorokin, K.D. Moiseev, V.A. Solov'ev, V. A. Kaygorodov, Ya.V. Terent'ev, B.Ya. Mel'tser, M.P. Mikhailova, Yu.P. Yakovlev, and P.S. Kop'ev, "3 μm Room Temperature Electroluminescence from Al(Ga)SbAs/InAs/Cd(Mg)Se Heterostructures with a Strong Carrier Confinement", Abstracts of Int. Workshop "Middle Infrared Coherent Sources", St. Peterburg, Russia, 51 (2001)
11. S.V. Ivanov, A.A. Toropov, I.V. Sedova, V.A. Solovyev, Ya.V. Terentyev, V.A. Kaygorodov, M.G. Tkachman, P.S. Kop'ev, and L.W. Molenkamp, "MBE Growth and Luminescence Properties of Hybrid Al(Ga)Sb/InAs/Cd(Mg)Se Heterostructures", Abstracts of XI^{th} Int. Conf. on MBE, Beijing, China, 226 (2000)
12. T.V. L'vova, I.V. Sedova, K.L. Kostushkin, S.V. Sorokin, V.P. Ulin, V.L. Berkovits, and S.V. Ivanov, "Surface morphology and chemical properties of InAs (001) substrates passivated by Na_2S water solutions", Abstract XXVI Workshop on Compound Semiconductor Devices, Chernogolovka, Russia, 67 (2002)
13. S. Ivanov, S. Sorokin, K. Moiseev, V. Solov'ev, V. Kaygorodov, Ya. Terent'ev, B. Meltzer, A. Semenov, M. Mikhailova, Yu. Yakovlev and P. Kop'ev, "Asymmetric hybrid

Al(Ga)SbAs/InAs/Cd(Mg)Se heterostructures for mid-IR LEDs and lasers", Proceedings of MRS Symposium H, Boston, MA, USA, 26-29 November, 2001, PM H8.8

14. A.N. Semenov, V.A. Solov'ev, B.Ya. Meltser, V.S. Sorokin and S.V. Ivanov, "Group V compositional control in Molecular Beam Epitaxy of AlGaAsSb alloys", Abstracts of XXX International School on the Physics of Semiconducting Compounds "Jaszowiec 2001", June 1-8, 2001, Ustron-Jaszowiec, Poland, Mo-25
15. A.N. Semenov, V.A. Solov'ev, B.Ya. Mel'tser, V. S. Sorokin, S.V. Ivanov and P. S. Kop'ev, "Anion Incorporation in AlGaAsSb Alloys Grown by MBE", Proceedings of 9th Int.Symposium "Nanostructures: Physics and Technology", St. Peterburg, Russia, 78 (2001).
16. Yu. P. Yakovlev (invited paper) "Novel III-V/II-VI mid-infrared laser structures with high asymmetric band offset confinements", MIOMD-IV, Montpellier, France, April 1-4, 2001
17. Yu.P. Yakovlev, S.V. Ivanov, K.D. Moiseev, A.M.Monakhov, V.A. Solovèv, I.V. Sedova, Ya.V.Terent'ev, A.A. Toropov, M.P. Mikhailova, B.Ya. Meltzer and P.S. Kop'ev "Novel hybrid III-V/II-VI mid-infrared laser structures with high asymmetric band offset confinements" SPIE Photonic West Conference, In-plane Lasers Section, San-Jose, USA, January 2002